FACULTY OF SCIENCE AND TECHNOLOGY

MASTER THESIS

Study programme / specialisation:
Petroleum Engineering/Drilling and Well Engineering

The spring semester, 2022

Open

Author:
Arsalan Royaei

.....
(signature author)

Course coordinator:
Rune Wiggo Time

Supervisor(s):
Rune Wiggo Time
Andrianifaliana Herimonja Rabenjafimanantsoa
Maryam Ghorbani

Thesis title:
Experimental Study of Displacement Flow of Miscible Fluids with Density Contrast in a Vertical, Concentric Annulus with Relevance to Reverse Cementing Technology

Credits (ECTS):
30

Keywords:
Primary cementing, Reverse and conventional circulation cementing, Unstable and stable density displacement, Fluid instabilities, Heavy over light displacement, Flow velocity, Atwood number, Concentric and eccentric annulus

Pages: 52

+ appendix: 28

Stavanger, 13.06.2022
date/year

UNIVERSITY OF STAVANGER

Experimental Study of Displacement Flow of Miscible Fluids with Density Contrast

in a Vertical, Concentric Annulus with Relevance to Reverse Cementing Technology

By:
Arsalan Royaei

June 13, 2022

Abstract

The primary cement job is an essential and complex operation in the oil and gas industry which is performed to support the casing, build a well barrier, and produce an isolated zone. Complete displacement of the drilling mud by cement without any contamination is critical for the productivity life of the well. The primary cementing consists of two methods. First is the conventional method, in which cement is pumped into the casing and turned back through the annulus. The second is the reverse method, in which cement is pumped into the annulus and back through the pipe, especially recommended for fractured zones and circulation loss problems. In recent years, there have been several studies related to the conventional cementing job, which is stable displacement. However, insufficient knowledge about the heavy-over light fluid displacement in reverse cementing prevents further improvement in the primary cementing process.

In this work, an experimental setup for reverse and conventional circulation in an annulus has been built and designed. Moreover, the unstable-density-displacement of two miscible fluids has been studied. Both fluids are Newtonian and low viscous. The main focus is studying the effect of flow velocities and density ratio between displaced and displacing fluids on displacement time and front velocity. More than 100 experimental runs have been done to analyze the different parameters. Water is considered as the light fluid, and for heavy fluid, salt (NaCl) is used as a weighting agent to increase and change the density of water. The heavy fluid is placed above the lighter fluid. Two fluids are initially separated by a ball valve. Also, an outlet valve is considered to regulate the flow velocity. The experimental runs are performed at Atwood numbers of 0.003 and 0.02 and flow velocities of 0, 12, 25, and 33 mm/s. Also, stable-density displacement has been studied for the Atwood number of zero (iso-dense fluids) and 0.02 to compare with unstable-density displacement. The fluid displacement is recorded by a camera, and videos are converted to images by a Python script. The spatiotemporal diagram is used to show the extension and development of the fluid mixing zone. The investigation of fluid displacement at different density ratios shows that there is a strong tendency to backflow and transverse flow for all unstable-density displacements. Also, the front velocity and mixing zone are increased with rising density instability. It is observed that the flow velocity and density difference affect the degree of instabilities. By increasing the imposed velocity, the backflow is suppressed, and the Atwood number's effect is weakened. Compared to unstable-density displacements, there is no backflow and transverse flow in stable-density displacement, and the displacing and displaced fluids are separated by a sharp interface. Although this interface is less clear for iso-dense displacement compared to the Atwood number of 0.02, the flow displacement is still uniform.

Acknowledgements

I would like to express my gratitude to my supervisor, Rune Wiggo Time, and co-supervisors, Andrianifaliana Herimonja Rabenjafimanantsoa and Maryam Ghorbani, for their valuable advice and constructive guidance, and commitment throughout my work on this thesis.

I am also highly appreciative and thankful to my family, especially my lovely wife, for so much devotion, care, and blessings.

Table of Contents

List of Tables

List of Figures

Nomenclature

A	**C**orrectional areal
At	**A**twood number
D	**D**iameter of pipe
Fr	**F**roude number
g	**G**ravitational constant
ID	**I**nner Diameter
L	**L**ength
m	**M**ass
OD	**O**uter Diameter
P,p	**P**ressure
Q	**F**lowrate
Re	**R**eynolds number
T,t	**T**ime
v	**V**elocity of Fluid
V	**V**olume
ρ	**D**ensity of Fluid
ρ**H**	**D**ensity of Heavy Fluid
ρ**L**	**D**ensity of Light Fluid
μ	**V**iscosity of Fluid
μ**H**	**V**iscosity of Heavy Fluid
μ**L**	**V**iscosity of Light Fluid

Abbreviations

CCCPT	**C**onventional Cement Circulation Placement Technique
HOL	**H**eavy Over Light
KHI	**K**elvin-Helmholtz Instability
RTI	**R**ayleigh-Taylor Instability
RCCPT	**R**everse Circulation Cement Placement Technique

Dedicated to my beloved family, for their perpetual love, support, and sacrifice, and to my wife, Nazanin, for her being the sounding board and the catapult in the trajectory of my life.

Chapter 1

Introduction

Displacing a light fluid with a heavier fluid exists in nature [1], as well as different industrial operations such as cementing operations in petroleum engineering. In this study, the reverse cementing is modeled experimentally, and the heavy over-light displacement of Newtonian fluids in a vertical and concentric annulus is investigated. Chapter one presents the cementing operation briefly. Moreover, it deals with previous research, limitations, and objectives. The chapter is closed with an overview of the thesis.

1.1 Background

A primary cement job is a significant and complex procedure in drilling a well in the oil and gas industry. The objective is to fill the gap between casing and wellbore with cement to produce an isolated zone, protect the casing from corrosion, preserve utilizable water, and prevent any uncontrolled flow from the reservoir to the annulus.

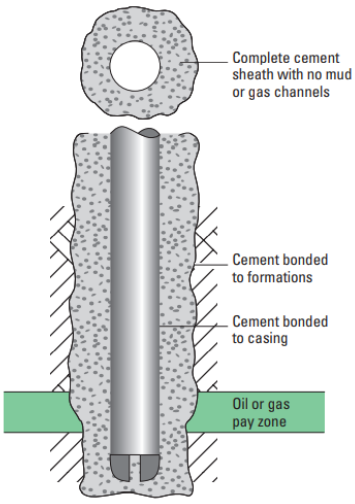

FIGURE 1.1: Purposes of primary cementing [2]

Uncontrolled flow can cause considerable problems such as a kick and environmental threats. To avoid these problems, primary cementing must make a hydraulic seal in the annulus between casing and formation as shown in Figure 1.1 [2].
There are two alternatives for primary cementing, namely, the conventional cement circulation placement technique (CCCPT) and the reverse circulation of cement placement technique (RCCPT). In conventional cement circulation, cement is pumped down to the casing and turned back through the annulus. This will be a challenging operation if there is a circulation loss, especially in the fractured zone. In this situation, it is recommended to pump cement slurry into the annulus directly and have it back through the casing using the reverse circulation technique to tackle the problem of circulation loss. Table 1.1 shows some advantages and disadvantages of the reverse method [3].

TABLE 1.1: Some advantages and disadvantages of reverse cementing operation [3]

Advantages	**Disadvantages**
ECD is reduced	Need extra design
Decrease the amount of cement for operation	Drilling fluid properties is more crucial
Reduce the placement time	May need backpressure on casing
Increase the safety and environmental control	More tools and kits are needed in RCCPT job
Reduce in using the retarders	Experience

Several studies have been performed in recent years on stable displacement, which is the conventional cementing method. However, the knowledge gap around the unstable displacement in reverse cementing jobs is a barrier to improving the primary cementing process. This thesis models the experimental heavy over light displacement and investigates different factors to design the reverse cementing technique better.

1.2 Literature review

In a primary cement job, mixing cement and mud can make channels and reduce the quality of the cement. Therefore, a steady displacement is crucial, which can minimize this mixing zone and prevent residual drilling mud. For this reason, the efficiency of displacing the drilling fluid with cement without contamination has been an essential topic in recent years. Different parameters affect fluid displacement like

fluid properties, flowrate, eccentricity, and inclination of the well [4].
The effect of the inclination is studied by T. Séon et al. [5]. The mentioned study showed that the front velocity of the interface is altered by changing the inclination. As it can be seen in Figure 1.2 from their experiments, for vertical pipe (θ=0), the front position between two fluids is not clear and challenging to be specified. By increasing the angle of inclination, three different regions are created. In region 1, the front position moves faster by inclination rise between 5° and 65°. In this region, transverse flow and segregation grow as well. The segregation between two layers of fluids becomes more visible in region 2, between the angle of 65° and 82°, and the front velocity reaches a plateau at the approximate maximum value. Finally, velocity is reduced for θ>82°.

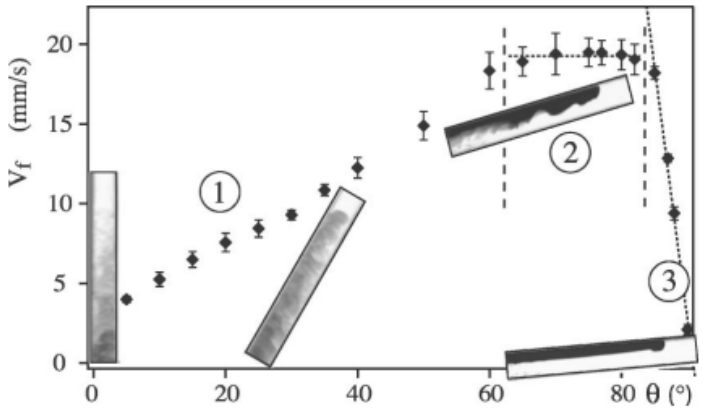

FIGURE 1.2: Front velocity as a function of the tilt angle (θ) [5]

In terms of the viscosity assessment, the density-unstable displacement flow of two miscible viscous fluids along an inclined pipe is presented by Ali Etrati et al. [6], where the heavier displacing fluid is on the top of the displaced fluid. The experiment results show that the viscosity ratio considerably impacts displacement efficiency. The efficiency is improved by making the displacing fluid viscous, but the efficiency is decreased by making the displaced fluid more viscous.
Malekmohammadi et al. [7] studied the effect of viscosity and eccentricity in a conventional cementing, which is density stable. They presented an experimental study of laminar miscible displacement flow in the vertical eccentric annulus in which heavy fluid displaced light fluid upward. They demonstrated that getting a steady traveling wave with an eccentric annulus is feasible. Also, a positive ratio of viscosity and density in a low eccentric annulus, meaning displacing fluid is more viscous and heavier than the displaced fluid, can improve the steadiness. Eccentricity provides a stronger azimuthal counter-current flow over and under the interface, which causes displacing fluid moves to the broader side of the annulus.
Hanieh K. Foroushan et al. [8] also investigated different parameters which are effective in fluid displacement during a primary cement job. The same result is reported

by them, which shows that displacing fluid must have higher viscosity and density compared to displaced fluid. Additionally, they found that turbulent flow improves the removal of the displaced flow on the narrow side of the annulus. However, an effective displacement might not necessarily result in this displacement because of the larger mixing zone. It is generally hard to say whether turbulent flow improves the fluid displacement or not. Also, they mentioned that eccentricity deteriorates the efficiency of the fluid displacement. At the same time, in an inclined situation with buoyancy-dominated displacement, it can enhance the interface of the fluid by gravity force. In addition, displacement is improved by the motion of the inner pipe when fluid is stuck in the narrow side of the annulus.
Between 2002 to 2009, 26 reverse cementing jobs were performed onshore successfully on the West Coast of the United States, as reported by Hernández and Bour [9]. Also, in the Gulf of Mexico [10] and Canadian Beaufort Sea [11], offshore reverse cementing method has been executed.
Other studies in density unstable displacement which can be mentioned are [12], [13], [14], [15], and [16].

1.3 Limitation and objectives

This thesis focuses on the reverse cementing job or alternatively the heavy-over light displacement in the oil and gas industry. The experimental setup was built by Dr. Hermonja A. Rabenjafimanantsoa, Ph.D. student Maryam Ghorbani and me, inspired by former master student Camilla Bjørnsens's work. The setup is set as vertical and concentric. Also, the fluids are Newtonian and miscible with constant low viscosity. The density difference between heavy and light fluid is not that much. Although some fluids are non-Newtonian and immiscible with high viscosities in the actual well, they are not considered in this study. Also, the motion of the pipe is neglected. The objectives of the thesis are:

- To design and construct a transparent annulus flow loop for reverse and conventional circulation with the capability of changing the eccentricity and inclination of the annulus.
- To study the role of velocity and density in heavy over light fluids displacement.
- To estimate the front velocity and displacement time.
- To compare unstable-density displacement with stable-density and iso-dense displacement.

1.4 Thesis overview

This thesis consists of 5 chapters. Chapter 1 is an introduction. Chapter 2 presents the theory of the thesis which defines the design of an oil well, fluid properties, dimensionless numbers, fluid flow, fluid instabilities, and governing equations. Chapter 3 is the design and methodology of the experiment in detail and presents the different parts of the setup. Chapter 4 deals with experimental results and discussions. Conclusion and recommendations for future works are presented in chapter 5.

Chapter 2

Theory

Complete displacement of drilling fluid during the primary cement job in the completion phase of oil and gas wells is essential to make an isolated zone and well integrity. This operation can affect productivity and abandonment of the well in the future. Insufficient displacement provides many problems, such as cement degradation and channeling, which can cause improper primary cement operation. So, a wide-spreading study of the fluid displacement and properties is required for a better cementing job [17].

2.1 Design of the wellbore

An oil and gas well is drilled from the surface to the reservoir in different segments caused of the formations' characteristics. After drilling each section, a casing is run, and a cement job is performed. Cement is pumped into the gap between formation and casing, or casing and casing called the annulus, to prevent leakage in this area, as shown in Figure 2.1.

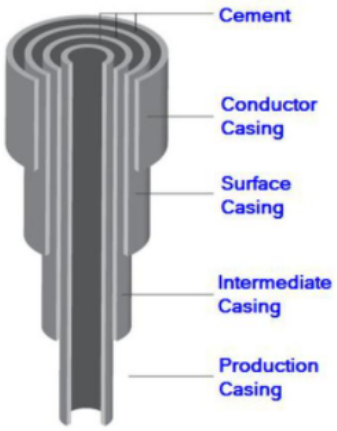

FIGURE 2.1: Schematic of a typical well

The goal is to place the cement behind the casing to ensure that there is an isolated zone and avoid the migration of the fluid into the well [18]. Some of the operational parameters that can affect displacement efficiencies, such as cementing techniques, deviation of the well, pipe eccentricity, and rotation of the pipe are mentioned below.

2.1.1 Cementing methods

Conventional circulation cementing and reverse circulation cementing are two techniques of primary cementing job which are used in the oil and gas industry. Figure 2.2A shows conventional methods in which cement is pumped down the casing and returned to the annulus. While in reverse cementing, cement is pumped down the annulus and circulated up through the casing. Figure 2.2B shows the schematic of reverse methods.

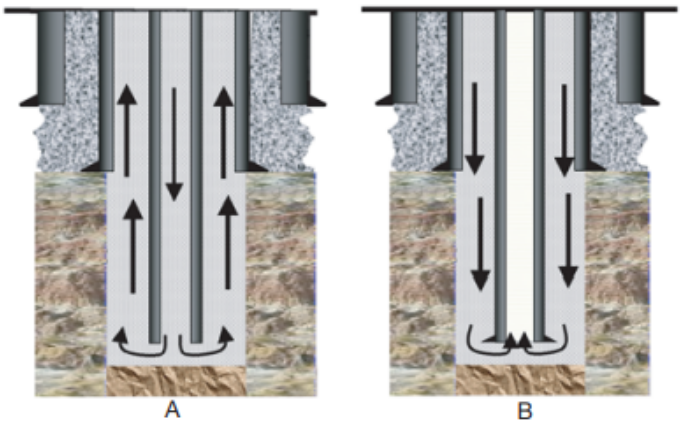

FIGURE 2.2: A) Conventional cementing method, B) Reverse cementing method [3]

The advantage of the reverse method is reducing the cement contamination, improving desired density and viscosity, and compared to the conventional method, the displacement volume and placement time are decreased [19].

2.1.2 Deviation of the well

Deviation of the well occurs when a wellbore deviates from the vertical direction. Some of the purposes of tilting the well or turning it to a horizontal direction are to cross the fracture zone, improve productivity, dig several wells from a single location, as well as be able to use it in multiple target zones [20]. There are some problems with conventional cementing jobs in a deviated or horizontal well like cutting transport, mud displacement, the eccentricity of the pipe, and a good hydraulic seal [8].
The inclination of the well affects the interface stability between cement and drilling mud. In a reverse cementing job for an inclined well, when cement with a higher density is located on the top of the drilling mud, three zones are formed due to the

instability, as shown in Figure 2.3. These three appeared zones are the transition zone which is related to the drilling mud, the exchange flow zone, and the transition zone, which is related to the cement [21].

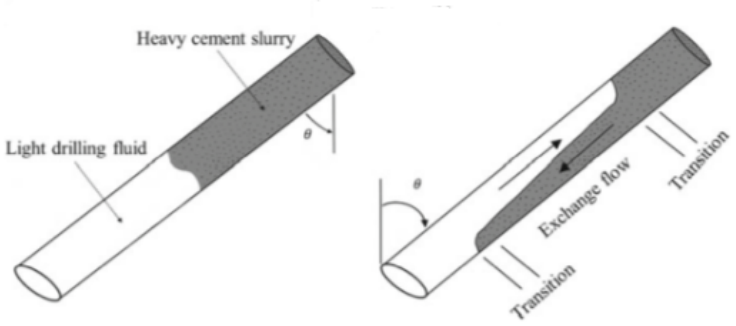

FIGURE 2.3: Effect of the inclination of the well on the fluid displacement [21]

2.1.3 Eccentricity of the well

A concentric annulus is when the pipe is centered in the casing or hole, while in an eccentric annulus, the pipe is not in the middle of the borehole. The pipe is not entirely concentric in natural wells because of the gravity force, and it affects the fluid flow. When the inner pipe is in contact with the outer pipe, eccentricity is 1, and the pipe standoff ratio is 100%. Additionally, for a concentric pipe, eccentricity is 0, and the standoff ratio is 0%. Figure 2.4 and Figure 2.5 show the standoff ratio and the effect of the eccentricity on the fluid displacement in the well, respectively [22].

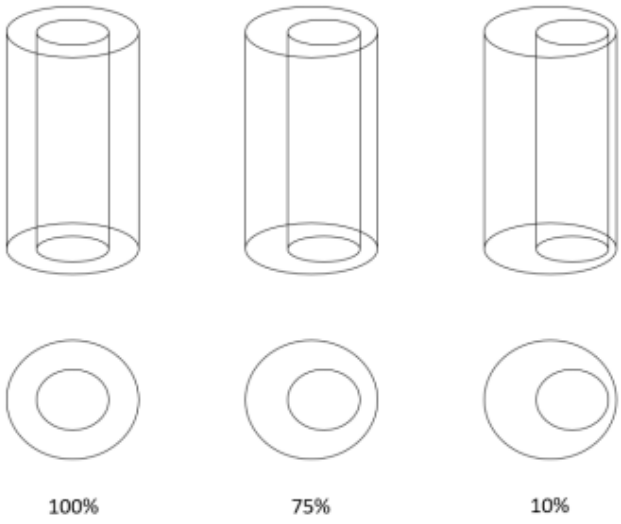

FIGURE 2.4: Schematic of eccentric annulus in a well

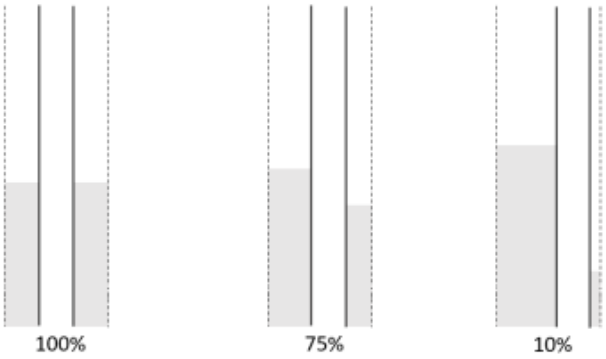

FIGURE 2.5: Effect of the eccentricity on upward fluid displacement

Considering the eccentricity is essential for designing the well, predicting casings, wearing drill string, and transporting the cutting. Equation 2.1 presents the relation between eccentricity and standoff ratio [2].

$$R_{STO} = [(1 - \epsilon) \times 100)] \tag{2.1}$$

Where:

R_{STO}= Standoff ratio
ϵ = Eccentricity

Eccentricity is one of the parameters that can affect the displacement of the fluid. In a concentric situation, cement seals perfectly because of the uniform annulus; however, cementing operation is more challenging in an eccentric annulus because fluid flows on the wider side of the annulus. Then, the mud channel can be found on the narrow side, which makes a poor cement bond between the casing and formation, as shown in Figure 2.6.

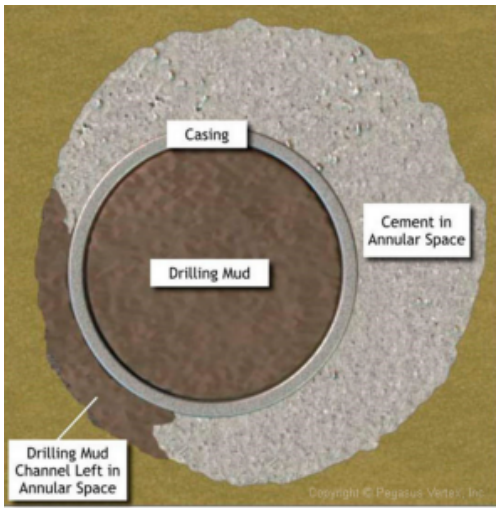

FIGURE 2.6: Mud channel on the narrow side of the annulus [8]

Also, this should be considered for setting the minimum flowrate to ensure adequate flow on the small side of the annulus [8].

2.1.4 Rotation of the pipe

Movement and rotation of the inner pipe during the cementing job can improve the displacement of the mud. Especially in an eccentric annulus, the movability of the fluid on the narrow side of the annulus is enhanced due to the rotation of the inner pipe, and total displacement efficiency is upgraded [8].

2.2 Fluid properties

2.2.1 Density

Density is defined as the ratio of the mass (m) per the volume (V) of a body, and it is shown by ρ. When discussing fluid displacement, density plays a vital role in fluid properties. In heavy over light displacement, the fluid with a higher density is identified as a" heavier" fluid that can displace a fluid with a lower density called a" lighter" fluid due to gravity. For instance, cement slurry is usually heavier than drilling mud since it has a higher density. Equation 2.2 shows the formula for the density. The unit of the density in SI is $kg/m3$.

$$\rho = \frac{m}{v} \tag{2.2}$$

The density of fluid changes with temperature; for instance, water has the highest density at 4°C. Also, salinity plays an essential role in the density of the water. With increasing the salinity, the density of the water is increased [23].

2.2.2 Viscosity

Viscosity is the resistance of a fluid to flow or deformation. Regarding the displacement of the fluid, when a pump with constant pressure is used, the liquid with lower viscosity has a higher flowrate due to lower internal force. For instance, a high viscose fluid, such as honey, flows slower than a less viscous fluid like water. Also, the viscosity of the fluid is decreased by increasing the temperature. Equation 2.3 shows viscosity formula based on shear stress τ and shear rate γ:

$$\mu = \frac{\tau}{\gamma} \tag{2.3}$$

The unit of the viscosity in SI is $N.s/m2$ or $Pa.s$ [24].

2.3 Dimensionless numbers

2.3.1 Reynolds number

The Reynolds number is defined as the ratio of inertial forces to viscous forces. It is a dimensionless number to identify the fluid's regime. Equation 2.4 shows the formula for the Reynolds number:

$$Re = \frac{\rho.v.d}{\mu} = \frac{inertia force}{viscose force} \tag{2.4}$$

Where:

ρ = fluid density $(\frac{kg}{m^3})$
v = fluid velocity $(\frac{m}{s})$
d = diameter of the pipe (m)
μ = fluid viscosity $(\frac{N.s}{m^2})$

The Reynolds number is used to specify whether fluid is in a laminar or turbulent flow. When inertia force is more than viscous force, the flow tends to be turbulent while viscose force is more dominated in a laminar flow. Flow inside pipes is categorized into three main regimes [25]:

Laminar flow : Re < 2000
Transient Flow : 2000 < Re < 4000
Turbulent flow : Re > 4000

Figure 2.7 shows the schematic of the laminar and turbulent flow.

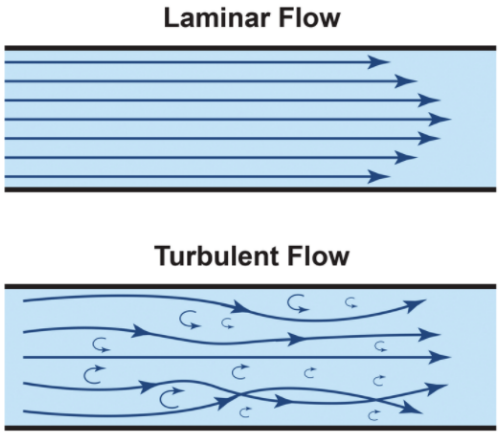

FIGURE 2.7: Schematic of Laminar and Turbulent flow

2.3.2 Atwood number

Atwood number is the density difference between two fluids. It is a dimensionless number and a significant parameter in instabilities, such as Rayleigh-Taylor. It can affect falling down the heavy fluid into light fluid and moving up the light fluid through the heavy fluid. Equation 2.5 shows the Atwood number formula [26]:

$$At = \frac{\rho_1 - \rho_2}{\rho_1 + \rho_2} \tag{2.5}$$

Where:

ρ_1 = density of the heavier fluid
ρ_2 = density of the lighter fluid

2.3.3 Froude number

The Froude number is dimensionless, and it depends on the fluid dynamic problems. It is defined as a ratio of inertia and effective gravitational forces. Equation 2.6 describes the densimetric Froude number formula [27]:

$$Fr = \frac{v}{\sqrt{Atg_{eff}D}} \tag{2.6}$$

Where:

Fr = Froude number
v = velocity ($\frac{m}{s}$)
At = Atwood number
g = acceleration of gravity (9.8 $\frac{m}{s^2}$)
g_{eff} = acceleration of gravity (g), compensated for inclination of flow
D = hydraulic mean depth or characteristic length (m)

When:

Fr = 1, critical flow
Fr > 1, supercritical flow (fast rapid flow)
Fr < 1, subcritical flow (slow/tranquil flow)

2.4 Fluid Flow

One of the significant parts of the cementing displacement is fluid flow. The nature and steadiness of the flow can affect the displacement. These are explained in the

following sections.

2.4.1 Natural and forced flow

Natural flow means fluid moves due to natural causes such as gravity or internal causes, for instance, buoyancy impact. In a heavy over light system, the displacing fluid has a higher density than the displaced fluid, and the flow moves downward from heavier fluid to lighter fluid naturally. Also, buoyancy can affect the flow based on the light fluid composition. In the forced flow, external sources such as a pump cause the flow; for instance, in cementing job, fluid flows to the well by a pump.

2.4.2 Steady state and unsteady state flow

In the steady-state flow, parameters do not change with time, while in unsteady-state flow, parameters such as pressure or energy change with time. As shown in Figure 2.8a for a steady displacement, the interface of the two fluids moves steadily, which causes the interface shape to not change along the displacement area. In contrast, Figure 2.8b shows an unsteady displacement in which the interface changes with time. The fluid moves faster on the broad side than on the narrow side.
Steady displacement in cement jobs decreases the mixing of the fluids, avoids mud challenge, and causes a continuous displacement of the drilling mud in the well [4].

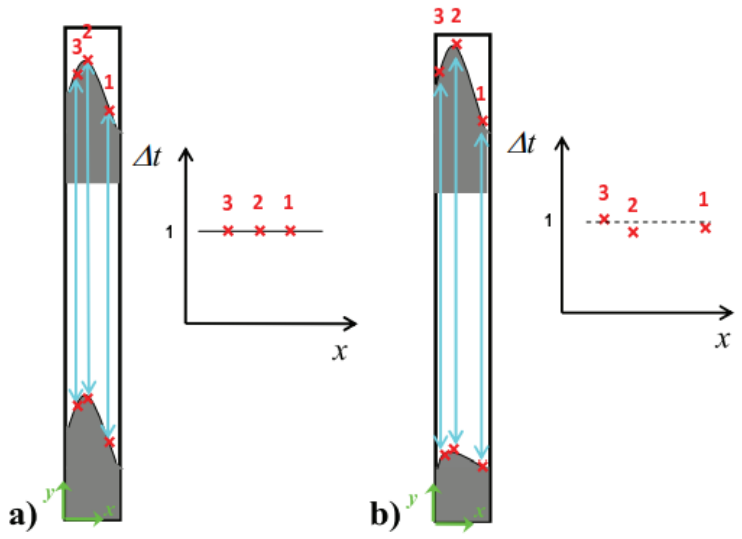

FIGURE 2.8: a) steady displacement b) unsteady displacement [28]

2.5 Fluid Instabilities

2.5.1 Kelvin-Helmholtz instability

The Kelvin-Helmholtz instability occurs when there are different velocities and densities at the interface of the two horizontal parallel flows. For instance, Figure 2.9 shows that the slight density difference between a cloud and the surrounding air causes Kelvin-Helmholtz instability [29].

FIGURE 2.9: Example of Kelvin-Helmholtz instability between a cloud and the surrounding air [29]

2.5.2 Rayleigh-Taylor instability

The Rayleigh-Taylor instability occurs when the heavier fluid is placed above the lighter fluid and is affected by gravity. Then, the interface between the two fluids becomes unstable because of the density difference [30]. For example, Figure 2.10 shows a planar laser-induced fluorescence (PLIF) picture of water at different temperatures. The density of water decreases with increasing the temperature due to the expansion. There is a slight density difference between the top layer at 17°C and the bottom layer at 22°C, and the flow direction is from left to right. The turbulent flow is formed when the lighter fluid rises into the heavy fluid, and the heavy fluid falls into the lighter fluid. The form of the RIT is illustrated in Figure 2.10, where a mushroom shape is formed by falling light-colored heavy fluid into the dark-colored light fluid [31].

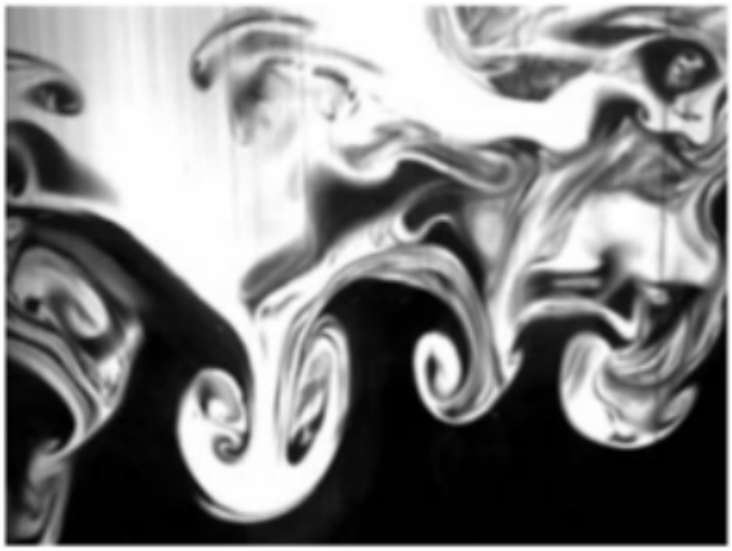

FIGURE 2.10: Mushroom shape in Rayleigh-Taylor instability [31]

2.6 Governing Equations of Fluid Dynamics

Computational Fluid Dynamics (CFD) is based on the conservation of mass, momentum, energy, and the fundamental laws used in fluid dynamics. The following sections define the quantity equation and Navier-Stokes equation related to the conservation of law and momentum, which are two crucial governing equations regarding fluid motion [32].

2.6.1 Quantity equation

The quantity equation is related to the conservation of mass. The movement or transport of a specified quantity is described by this equation, and it is defined as:

$$\frac{\partial \rho}{\partial t} + \nabla.(\rho \vec{u}) = 0 \tag{2.7}$$

Where:

ρ = density of the fluid
t = time
$\vec{u}$ = velocity vector of the fluid

For the homogenous and incompressible fluid, quantity equation is expressed as [32]:

$$\nabla.\vec{u} = 0 \tag{2.8}$$

2.6.2 Navier-Stokes equation

The Navier-Stokes equation is related to the motion of the fluid. For a Newtonian, incompressible viscous fluid, It is defined as [33]:

$$\rho(\frac{\partial \vec{u}}{\partial t} + (\vec{u}.\nabla)\vec{u}) = -\nabla p + \mu.\nabla^2\vec{u} + \rho\vec{g} \tag{2.9}$$

Where:

$\rho(\frac{\partial \vec{u}}{\partial t} + (\vec{u}.\nabla)\vec{u})$	: inertia force
∇p	: pressure force
$\mu.\nabla^2\vec{u}$	: viscous force
$\rho\vec{g}$	: hydrostatic pressure gradient

By rearranging equation 2.9, different dimensionless numbers can be derived, for example, the Atwood number, Reynolds number, and Froude number. $\overline{\rho}$ is considered the average density of the heavy and light fluid.

$$\overline{\rho} = \frac{1}{2}(\rho_1 + \rho_2) \tag{2.10}$$

Also, for heavy fluid (i = 1), Φ_i is equal to +1 and for light fluid (i = 2), Φ_i is equal to -1.

$$\rho_i = \overline{\rho}(1 + \Phi_i At) \tag{2.11}$$

The ratio of characteristic velocity scale (U_0) and dimensionless velocity vector ($\hat{\vec{u}}$) are shown in $\vec{u} = U_0\ \hat{\vec{u}}$ and characteristic length scale D_0 is defined in $x = D_0\ \hat{x}$. Moreover, timescale is defined as D_0/U_0 and pressure scale is shown by p_0. The Navier stokes equation can be written as:

$$\overline{\rho}(1 + \Phi_i At)\frac{U_0^2}{D_0^2}(\frac{\partial \vec{u}}{\partial t} + (\vec{u}.\nabla)\vec{u}) = -\frac{p_0}{D_0}\nabla p + \frac{\mu U_0}{D_0^2}\nabla^2 u + \overline{\rho}(1 + \Phi_i At)\vec{g} \tag{2.12}$$

By rearranging equation equation 2.12, equation 2.13 is derived :

$$(1 + \Phi_i At)\frac{\overline{\rho}U_0 D_0}{\mu}(\frac{\partial \vec{u}}{\partial t} + (\vec{u}.\nabla)\vec{u}) = -\frac{p_0 D_0}{\mu U_0}\nabla p + \nabla^2 u + \overline{\rho}(1 + \Phi_i At)\frac{D_0^2\vec{g}\overline{\rho}}{\mu U_0} \tag{2.13}$$

By considering equation 2.14 which is:

$$-\frac{\rho_0 D_0}{\mu U_0}\nabla p + \frac{D_0^2 \vec{g}\overline{\rho}}{\mu U_0} \rightarrow -\nabla p' \tag{2.14}$$

Where p_0 = $\frac{\mu_0 U_0}{D_0}$, p = p′ + $\frac{\vec{g}\overline{\rho}\vec{x}}{p_0}$ and Re = $\frac{\overline{\rho} U_0 D_0}{\mu}$, the Navier-Stokes equation becomes:

$$(1+\Phi_i At)Re(\frac{\partial \vec{u}}{\partial t} + (\vec{u}.\nabla)\vec{u}) = -\nabla p' + \nabla^2 \overline{u} + \Phi_i \frac{At D_0^2 \vec{g}\overline{\rho}}{\mu U_0} \tag{2.15}$$

If the last term of the equation 2.15 be written as $\frac{At g D_0}{U_0^2} \times \frac{\overline{\rho} U_0 D_0}{\mu}.\vec{e_g}$ where:

$\frac{1}{Fr^2}$ = $\frac{At g D_0}{U_0^2}$
$\vec{e_g}$ = unit vector for gravity

Finally, the Navier-Stokes equation included dimensionless numbers such as At, Re, and Fr becomes [34] [35]:

$$(1+\Phi_i At)Re(\frac{\partial \vec{u}}{\partial t} + (\vec{u}.\nabla)\vec{u}) = -\nabla p' + \nabla^2 \overline{u} + \Phi_i \frac{Re}{Fr^2}\vec{e_g} \tag{2.16}$$

Chapter 3

Design and Methodology

3.1 Design of the experimental Setup

The experimental setup has been built and designed for stable and unstable fluid displacement in the annulus with the ability to change the eccentricity and inclination of the pipe. It consists of a 2-meter long vertical acrylic pipe with a 40 mm inner diameter and a smaller multilayer composite pipe with a 25 mm outer diameter. The annular space between the pipes is 15mm. The pipes are seated inside a rectangular fish tank containing glycerol to decrease optical distortion and regulate the light deflection of acrylic walls. A ball valve is located half a meter from the top to separate the heavy and light fluids. The upper part is initially filled with heavy fluid, and lighter fluid is placed below the valve. A tube is connected at the bottom of the annulus, which leads the flow to the drain. There is a 1/4-inch outlet valve to control the velocity of the flow. A tank containing heavy fluid with a bilge pump is placed near the setup to continuously feed the heavy fluid from the top.

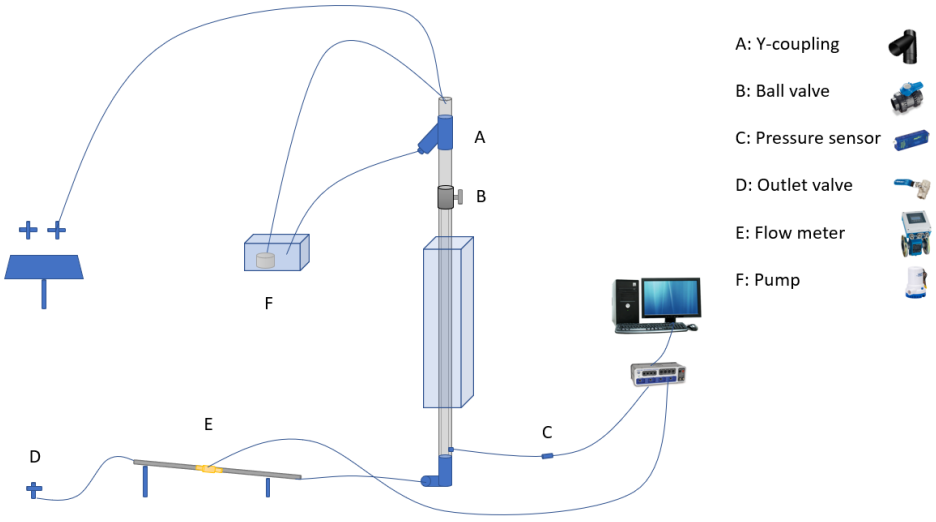

FIGURE 3.1: Schematic of the experimental Setup

Also, a 45°Y-coupling is located on the top to ensure the hydrostatic pressure and fluid height are constant during the experiment. A pressure sensor is installed at the bottom of the annulus, and an electromagnetic flowmeter is mounted before the outlet valve; both are connected to a computer using the PASCO interface to record the pressure and flowrate simultaneously. Figure 3.1 shows the schematic of the experimental setup.

3.1.1 Scaling

Table 3.1 shows the geometrical values for the experimental setup. The length of the pipe was selected by the relation of the axial length up to the valve, the hydraulic diameter, and the circumference, which seems to be sufficient to see the displacement's dominating effects.

TABLE 3.1: Geometrical values for the experimental setup

Parameter	**Symbol**	**Value**
Total height of the pipe	L+H	2m
Height up to ball valve	L	1.5m
Height above ball valve	H	0.5m
Inner diameter of the outer pipe	ID	40mm
Outer diameter of the inner pipe	OD	25mm
Hydraulic diameter	DH= OD-ID	15mm
Circumference of annulus	C=$\pi(ro + ri)$	102.1mm
Axial length/hydraulic diameter	L/DH	100
Axial length/circumference	L/C	14.69

As shown in Table 3.2, for the scaling of the experimental setup, the typical relation between the hole and the casing in the actual oil and gas well was considered to find the pipe's outer and inner diameter.

TABLE 3.2: Relation between hole section and inner casing in a typical oil well

Hole section (OD)	**Inner casing**	**Ratio**
$17\frac{1}{2}$ inches	$13\frac{3}{8}$ inches	1.3
$12\frac{1}{4}$ inches	$9\frac{5}{8}$ inches	1.27
$8\frac{1}{2}$ inches	7 inches	1.21

Table 3.3 displays that the inner diameter of the outer pipe is 40 mm, and the outer diameter of the inner pipe is 25 mm in the experimental setup, which gives a ratio of 1.6. This higher value compared to the typical oil and gas well was selected to visualize the annulus displacement better.

TABLE 3.3: Relation between inner diameter of the outer pipe and outer diameter of the inner pipe in the experimental setup

Outer pipe (ID)	**Inner pipe (OD)**	**Ratio**
40 mm	25 mm	1.6

Also, Table 3.4 depicts the range of the parameters which were considered for the displacement flow in this experiment.

TABLE 3.4: The range of the parameters for the experimental study

Parameters	**Symbol**	**Value**
Velocity	v	0-35 (mm/s)
Reynolds number	Re	0-527
Atwood number	At	0-0.02
Froude number	Fr	0-1.67

3.1.2 Camera system

A Nikon D5500 camera with 60 fps is selected to take the video of the fluid displacement. The camera is attached to the support system and placed in front of the setup. Also, a Python script is used to split the video into picture frames.

Visualization improvement

The fish tank is a rectangular tank filled with glycerol located around the pipe, which is designed to reduce the cylindrical effect and improve the quality of the picture. Black drawing ink is added to the displacing fluid to distinguish it from the displaced fluid and visualize the displacement better. Also, two mirrors are located on both sides of the setup to capture the fluid displacement on the left and right-hand sides and behind the pipe, as shown in Figure 3.2. The angle between mirrors and setup must be 45 degrees to ensure the size of the annulus in the mirrors is the same as the actual one. Four white curtains are placed around the setup to improve the natural background, and also, a white curtain covers the camera and the support system to avoid the reflection. An LED panel is located behind the pipe, and another one is placed in front of the setup on the floor to upgrade the lighting.

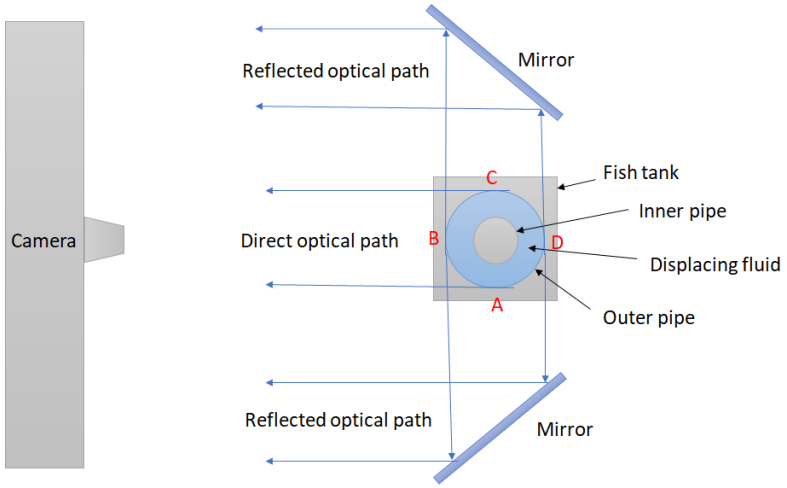

FIGURE 3.2: Schematic of the optical system

Black drawing ink is added to the heavy fluid to distinguish it from the lighter fluid and visualize the displacement better. Also, two mirrors are located on both sides of the setup to capture the fluid displacement on the left and right-hand sides and behind the pipe, as shown in Figure 3.2. The angle between mirrors and setup must be 45 degrees to ensure the size of the annulus in the mirrors is the same as the actual one. Four white curtains are placed around the setup to improve the natural background, and also, a white curtain covers the camera and the support system to avoid the reflection. An LED panel is located behind the pipe, and another one is placed in front of the setup on the floor to upgrade the lighting.

3.1.3 Inclination control

The experimental setup is built so that the inclination of the pipe can be changed. The pipe is fixed to a frame with the RS PRO Aluminum strut vertically, and a lever is attached to the frame at the bottom of the setup for tilting the pipe to provide different pipe inclinations (see Appendix C).

3.1.4 Eccentricity control

A connector is designed and built to control the eccentricity of the pipe and placed after the ball valve to remove the effect of the valve and make the flow uniform and straightened. Two connectors have been used for the sides of the pipe, and another small one is located in the middle of the pipe. The eccentricity can be modified by changing these connectors. Figure 3.3 shows these connectors for the end and middle of the pipe, which are designed to make the pipes concentric.
Other connectors have been designed and built to change the eccentricity. By replacing these connectors, the effect of the eccentricity can be investigated. Figure 3.4

shows the connectors designed to analyze the effect of the eccentricity of the pipe on fluid displacement.

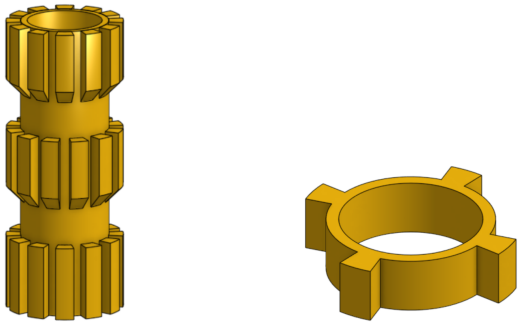

FIGURE 3.3: Connectors and flow straightener for concentric annulus

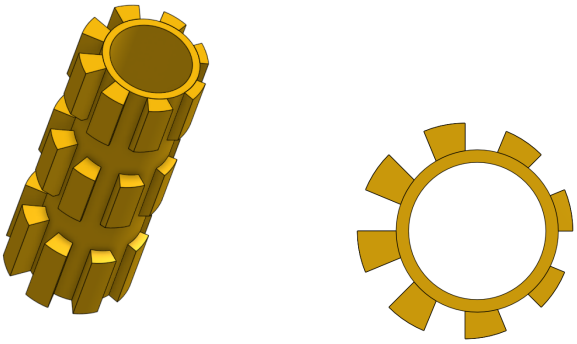

FIGURE 3.4: Connectors and flow straightener for eccentric annulus

3.1.5 Data acquisition

PASCO Capstone software is selected to measure pressure and flowmeter data. The pressure and flowmeter sensors are connected to a computer via an 850 Universal Interface, which is shown in Figure 3.1. Some examples of the Pasco graphs are shown in Appendix E.

Electromagnetic flowmeter

An Endress+Hauser Promag 53 Flowmeter is used for the experiments. It is an electromagnetic flowmeter with Faraday's law to measure the velocity of electrically conducting fluids. A coil system is located in the flowmeter and provides a magnetic field perpendicular to the flow direction. Two electrodes are mounted to measure the velocity by the voltage. Figure 3.5 shows that electrical voltage is produced by moving conductive fluid through the magnetic field. This electrical voltage is proportional to velocity [36]. The flowmeter is calibrated for the experiment and placed before the outlet valve (see Appendix A).

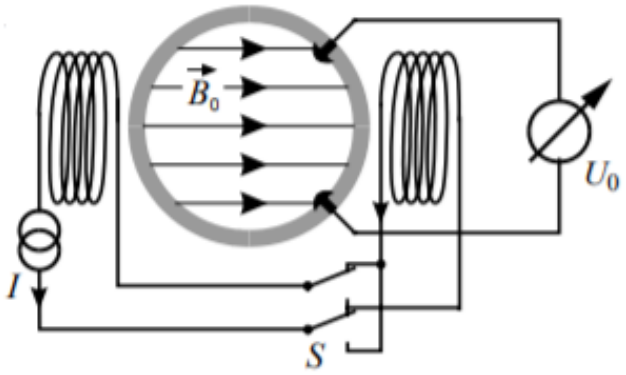

FIGURE 3.5: Magnetic fields in electromagnetic flowmeter

The flowmeter was shown an empty pipe error when it was in a completely horizontal position, as shown in Figure 3.6. This problem was solved by changing the outlet pipe's angle upward (see Figure 3.7).

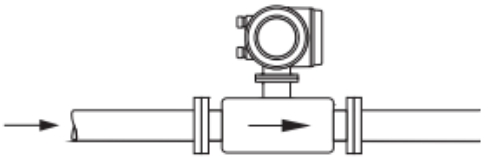

FIGURE 3.6: Flowmeter in horizontal position

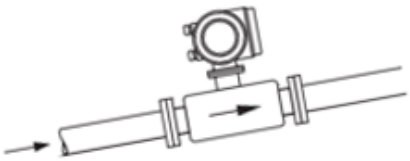

FIGURE 3.7: Flowmeter in inclined position

Pressure sensor

An absolute pressure sensor is used in this experiment and located at the bottom of the vertical pipe. It is connected to the Pasco interface with a VWR silicon tube. Also, it has been calibrated for the experiment (see Appendix A). Figure 3.8 illustrates the absolute pressure sensor and its connections.

FIGURE 3.8: Absolute pressure sensor and its connections

3.2 Selection of fluids

Water is considered an incompressible Newtonian fluid, which is selected as a light fluid in this experiment. For the heavy fluid, salt (NaCl) is used as a weighting agent to increase the density of water, and Glycerol is used to change the viscosity of the fluids if needed. As mentioned before, black ink is added to the displacing fluid to distinguish it from the displaced fluid.

3.2.1 Density meter

Figure 3.9 shows a density meter DMA 4500 M used to measure the fluid density. It consists of a U-shaped borosilicate glass tube. When the fluid sample is injected, the U-tube starts to vibrate, and its characteristic frequency is altered due to the density of the sample. After each sample, the density meter must be washed with fresh water and soap. Also, acetone is injected and pumped to dry the U-tube to be prepared for the next sample.

FIGURE 3.9: Density meter DMA 4500 M[37]

By Equation 3.1, the density of the sample is calculated.

$$\rho = KA.Q^2.f_1 - KB.f_2 \tag{3.1}$$

Where:

KA,KB = apparatus constants
Q = quotient of the period of oscillation of the U-tube divided by the period of oscillation of the reference oscillator
F_1,F_2 = correction terms for temperature, viscosity and nonlinearity

3.2.2 Viscosity meter

The flow properties of the fluid are specified by the OFITE Model 800 Viscometer based on shear stress and the shear rate at atmospheric pressure over different times and temperatures. There are eight test speeds : 3 (Gel), 6, 30, 60, 100, 200, 300, and 600, which are altered by a control knob, and shear stress is shown on a lighted magnified dial. Figure 3.10 shows a schematic of Model 800 Viscometer and its components [38].

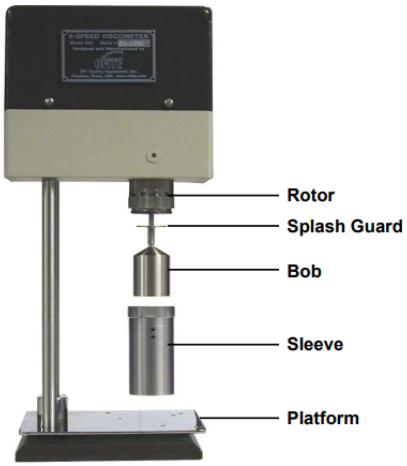

FIGURE 3.10: Schematic of viscometer and its components [38]

3.3 Experimental uncertainties

3.3.1 Flow velocity

Flow velocity is controlled by a small ball valve attached to the outlet pipe. It is challenging to set velocity at the specific value for all cases because the valve is controlled manually.

3.3.2 Eccentricity of the pipe

The connectors have been designed to straighten the flow and control the eccentricity to make the pipe concentric. Nevertheless, it is not easy to set the pipe completely in a vertical and concentric position, which can affect the flow displacement.

3.3.3 Valves opening

A slight difference in the opening time of the ball valve between heavy and light fluid and the outlet valve affects the mixing zone. Because the valves are opened manually by two people, it is challenging to do that simultaneously; however, this effect can be neglectable. Also, a flow straightener is placed after the ball valve, which acts as a honeycomb to decrease this effect.

3.3.4 Residual salt

Between the runs, the setup is washed down with fresh water to remove the residual ink and salt due to the heavy fluid in the pipe. But, It is supposed that the leftover salt that remains in the pipe can affect the light fluid's density for the next run. However, this small amount can be neglected.

3.3.5 Residual water

For starting the experiment, the pipe is filled with displaced fluid up to the ball valve to ensure there is no air between displacing and displaced fluid. The height of the fluid is controlled by the pressure sensor. After that, the ball valve is closed, and the pipe is filled with displacing fluid. It is not easy to control the leftover fluid above the ball valve for each run. Moreover, this fluid is mixed with the displacing fluid and changes the density.

3.4 Experimental method

At first, the outlet valve is closed, and the ball valve on the top of the annulus is open. The annulus becomes filled up to the ball valve with tap water as displacing fluid. The pressure sensor at the bottom of the annulus controls the height of the lighter fluid to ensure the fluid is above the ball valve, and it is the same for all runs. Then, the ball valve is turned off, and the rest of the annulus is filled with heavy fluid from a container using a bilge pump. It is better to open and close the ball valve several times to ensure that there is no bubble inside the valve. As it is mentioned earlier, the pump is feeding the annulus with heavy fluid, and a 45° Y-coupling on top of the pipe ensures the fluid height is not rising by flowing fluid back to the heavy fluid tank. For starting the experiment, both ball and outlet valves are opened simultaneously to ensure the flow. The flow velocity is adjusted by regulating the outlet valve. PASCO software measures the pressure and flowrate, and a camera records a video of the area of interest during the experiments. When the heavy fluid displaces all the lighter fluid, the recording is stopped. The pump is turned off, and the setup is washed with fresh water to ensure no residual denser fluid is left in the annulus for the next

experimental run.
The procedure is the same for stable-density displacement. The difference is that the annulus is filled with heavy fluid initially, and the lighter fluid is placed above the heavy fluid.

3.5 Experimental plan

The experimental plan is summarized in Table 3.5. Experimental runs in series 1 and 2 represent stable-density displacement. In series 1, light fluid is located above the heavy fluid, and the effect of the flow velocity is investigated for At = 0.02. In series 2, experimental runs are done on iso-dense fluid displacement in which the density of the displacing and displaced fluids are the same. These series are considered to compare with unstable-density displacement. The light fluid density is constant in series 3 and 4 and placed under the heavy fluid. In contrast, the density of the heavy fluid is changed to get different Atwood numbers. The effect of the different fluid velocities is analyzed for each Atwood number. Also, displacement time and front velocity are studied.

TABLE 3.5: Experimental plan

Series	**Displacing fluid density (gr/cm3)**	**Displaced fluid density (gr/cm3)**	**Atwood number**	**Velocity range (mm/s)**
1	0.998	1.038	0.02	12,25,33
2	0.998	0.998	0	12,25,33
3	1.005	0.998	0.003	0,12,25,33
4	1.038	0.998	0.02	0,12,25,33

Chapter 4

Results and Discussions

4.1 Experimental variables

Table 4.1 to Table 4.4 show the experimental test matrix. The variables are Atwood number and imposed velocity. Atwood number shows the effect of the density ratio, Reynolds number is proportional to the fluid velocity, and Froude number includes the effect of fluid velocity and density difference. There are two runs at each velocity to prove the repeatability of the results.

TABLE 4.1: Overview of the experimental variables for stable-density displacement, At = 0.02

Series	Voltage (v)	v (mm/s)	Re	Fr	Re/Fr
1.0.1	1.22	12.5	188	0.23	813.7
1.0.2	1.21	11.6	174	0.21	813.7
1.1.1	1.35	24.2	364	0.44	813.7
1.1.2	1.36	25.1	378	0.46	813.7
1.1.1	1.46	34.2	513	0.63	813.7
1.2.2	1.45	33.3	500	0.61	813.7

TABLE 4.2: Overview of the experimental variables for stable-density displacement, At = 0

Series	Voltage (v)	v (mm/s)	Re	Fr	Re/Fr
2.0.1	1.22	12.5	188	-	-
2.0.2	1.21	11.6	174	-	-
2.1.1	1.36	25.1	378	-	-
2.1.2	1.35	24.2	364	-	-
2.2.1	1.46	34.2	513	-	-
2.2.2	1.45	33.3	500	-	-

TABLE 4.3: Overview of the experimental variables for unstable-density displacement, At = 0.003

Series	Voltage (v)	v (mm/s)	Re	Fr	Re/Fr
3.0.1	0	0	0	0	-
3.0.2	0	0	0	0	-
3.1.1	1.21	11.6	174	0.55	315.1
3.1.2	1.22	12.5	188	0.59	315.1
3.2.1	1.36	25.1	378	1.19	315.1
3.2.2	1.35	24.2	364	1.15	315.1
3.3.1	1.47	35	527	1.67	315.1
3.3.2	1.45	33.3	500	1.58	315.1

TABLE 4.4: Overview of the experimental variables for unstable-density displacement, At = 0.02

Series	Voltage (v)	v (mm/s)	Re	Fr	Re/Fr
4.0.1	0	0	0	0	-
4.0.2	0	0	0	0	-
4.1.1	1.21	11.6	174	0.21	813.7
4.1.2	1.22	12.5	188	0.23	813.7
4.2.1	1.35	24.2	364	0.44	813.7
4.2.2	1.36	25.1	378	0.46	813.7
4.3.1	1.45	33.3	500	0.61	813.7
4.3.2	1.46	34.2	513	0.63	813.7

Setting the same voltage and getting the same velocity for each run is difficult because the outlet valve is adjusted manually, but it is reasonably similar. Since salt is added to water to increase the density, a small variation in the amount of water and salt can change the density. However, this difference in the Atwood number is negligible.
The voltage is converted to fluid velocity using the calibration equation 4.1 of the flowmeter (more details can be found in Appendix A).

$$v = 90.237V - 97.078 \tag{4.1}$$

Where:

v = fluid velocity (mm/s)
V = voltage (v)

4.2 Post processing

Figure 4.1 illustrates the annulus and two mirrors installed to cover the 360-degree of the annulus in the azimuthal direction. The front side of the annulus (A.B.C in Figure 3.2) is marked by (a) in Figure 4.1. (b) shows the left side of the annulus (B.C.D in Figure 3.2) in the mirror , and the right side (B.A.D in Figure 3.2) is shown by (c) in Figure 4.1.

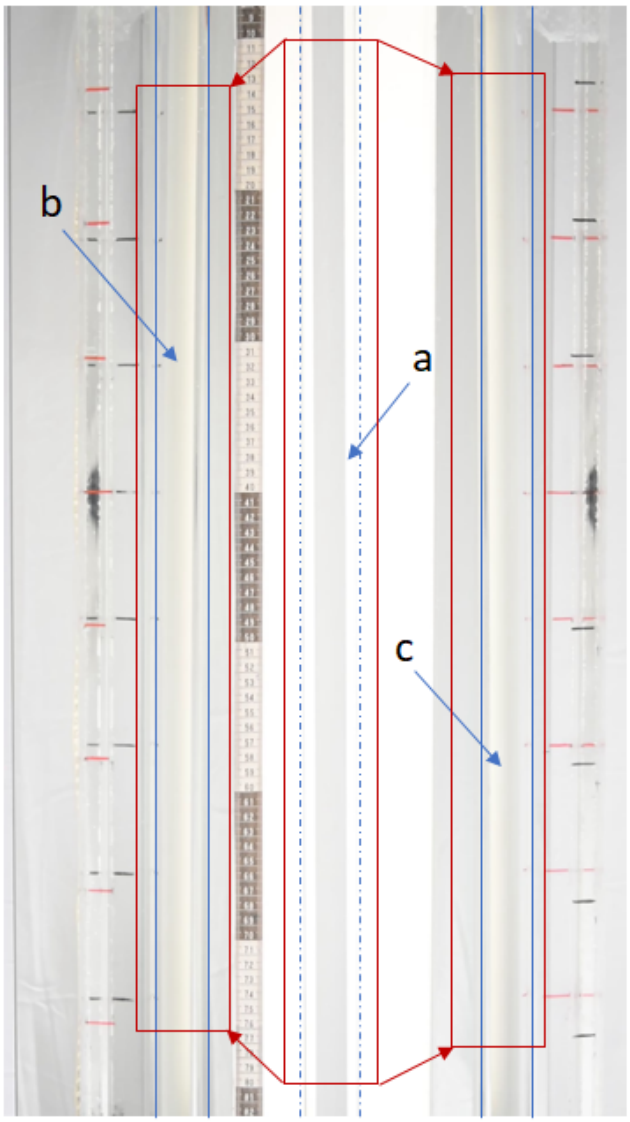

FIGURE 4.1: Visualization of the displacement.
(a) front view of annulus, (b) left side of annulus in mirror, (c) right side of annulus in mirror

A scale has been installed on the front side of the fish tank to find the equivalent images of the specific area of the annulus in the mirrors. Red and black horizontal lines have been marked on the left and right sides of the fish tank, each 10 cm. Based on this scale and these markers, the red rectangles in Figure 4.1 show 70 cm of the

annulus and the equivalent images in the left and the right mirrors.
For the image processing, some scripts in python provided by Ph.D. student Maryam Ghorbani have been used.

4.2.1 Spatiotemporal diagram

First, the frames at different time steps are extracted from the videos of the experiments, and then in each frame pixel is converted to the meter unit using the scale installed on the fish tank. The grey scaled images are used. The maximum value of the darkness is considered as the concentration of 1 to scale the darkness of images in the range of zero to 1. The value of zero shows the concentration of the light fluid, and 1 represents the heavy fluid. The concentration in between shows the mixing zone. The spatiotemporal diagram is used to illustrate the extent and evolution of the fluid mixing zone. In these diagrams, in each time step, the fluid concentration is averaged in horizontal cross-sections (which is equivalent to radial and azimuthal averaged values) along the annulus. The images in mirrors are used as they have covered 360 degrees of the annulus. Figure 4.2 is given as an example of these diagrams. The light color and concentration of 0 is lighter fluid, and the black color shows the heavy fluid which is supplied from the top. During the time interval shown in this diagram, the front of the heavy fluid has reached the bottom. The blended colors show the mixing region during the displacement.

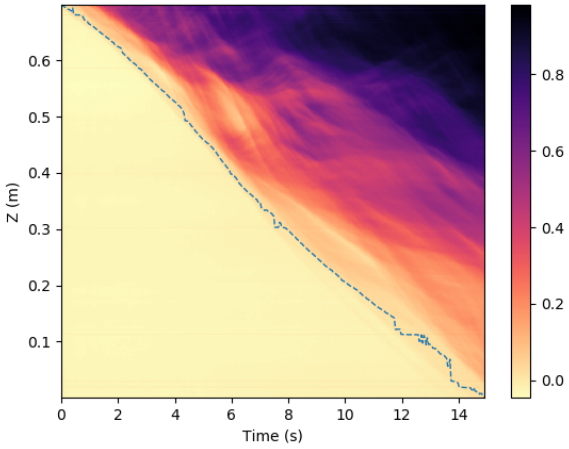

FIGURE 4.2: Spatiotemporal diagram for At = 0.02 and v = 12 mm/s

One parameter which has been studied is the velocity of the front position and the growth of the mixing zone.

4.2.2 Front velocity

In Figure 4.2 dashed line shows the front position separating pure light fluid from the mixing region. Throughout this study, the mixing zone is defined as the flow region

where the concentration is more than 0.02. To calculate the front velocity, the slope of this line is considered.

4.2.3 Displacement time

Another parameter considered in this study is the time of the fluid displacement. The time taking the light fluid is displaced completely by the heavy fluid is introduced as the displacement time. The start of displacement is when the heavy fluid has entered the annulus (Concentration> 0), and the end of displacement is when the outlet is fully filled with the heavy fluid (Concentration> 0.97). Another script in python is used to calculate this parameter. Figure 4.3 shows this parameter for the case of Atwood number of zero and velocity of 25 mm/s as an example. The blue curve shows the concentration change at the inlet, and the red one illustrates the concentration over time at the outlet. The dashed lines show the times of the start and end of displacement and when the inlet is fully filled with the heavy fluid.

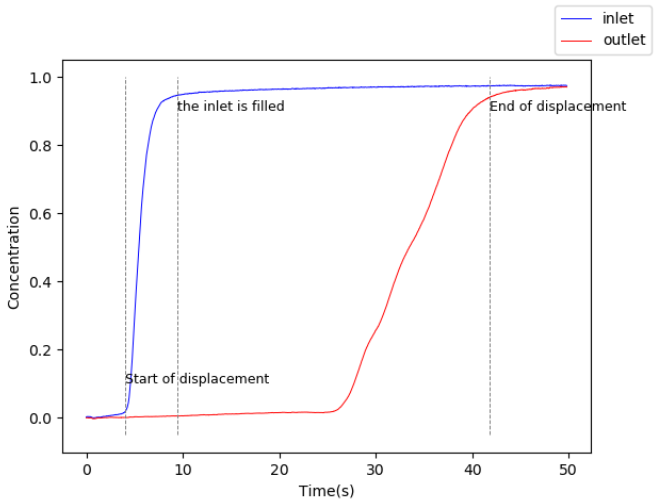

FIGURE 4.3: Displacement time for At = 0 and v = 25 mm/s

4.3 Example of a typical displacement

This section discusses the fluid displacement with the Atwood number of 0.003 and the imposed velocity of 12 mm/s as an example. The front and side views of the annulus at different time intervals are presented in the Figure 4.4. The fluid displacement over time can be seen in this figure. The annulus is initially filled with the light fluid, and the heavier fluid is injected from the top to displace the lighter one. Because of density instability, there is not a clear interface between two fluids. There is a lot of instability, a tendency to backflow, and transverse flow because of the growth of Rayleigh-Taylor instability.

(a) The left side of the annulus in the mirror

(b) The front side of the annulus

(c) The right side of the annulus in the mirror

FIGURE 4.4: Fluid displacement for At = 0.003 and v = 12 mm/s

Moving the displaced fluid upward against the imposed flow is called backflow, which is observed during the displacement. Also, swirling the fluid around the annulus is called transverse flow. Both are shown in Figure 4.5.

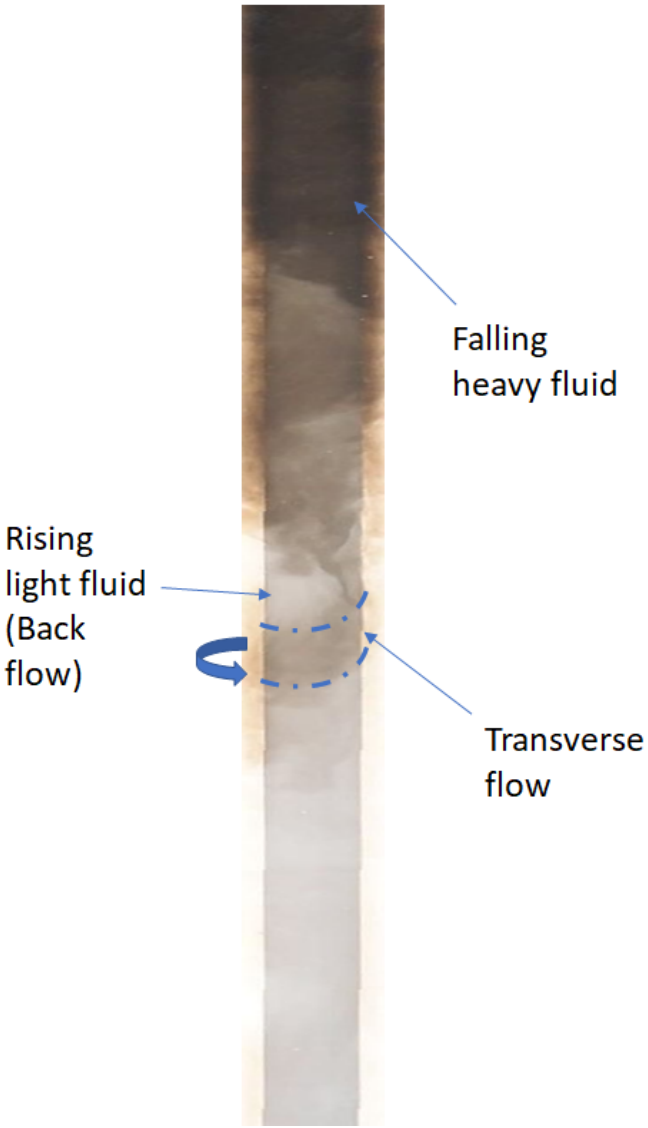

FIGURE 4.5: Example of flow patterns during the fluid displacement

4.4 Effect of flow velocity

The effect of the flow velocity at different ranges of density ratio is investigated in this section.

4.4.1 Stable-density displacement

In stable-density displacement, the displacing fluid is not denser than the displaced fluid. For these cases, imposed velocities are 12, 25, and 33 mm/s, and as they are density stable, running an experiment without imposed velocity (no flow) does not make sense.

At = 0.02 with heavy fluid at the bottom

In this case, the pipe is filled with heavy fluid, and lighter fluid is injected from the top. Black ink is added to the displacing (light) fluid to distinguish it from the displaced fluid. The spatiotemporal diagrams for different flow velocities at Atwood number of 0.02 are shown in Figure 4.6. It is clear that displacement time is decreased, and front velocity is increased by increasing the flow velocity. The flow pattern along the annulus during the displacement for this case is given in Figure 4.7. The figures confirm that the setup is sufficiently vertical and concentric. There is no backflow and transverse flow. Two fluids are separated by a sharp interface. The shape of this interface is steady during the displacement.

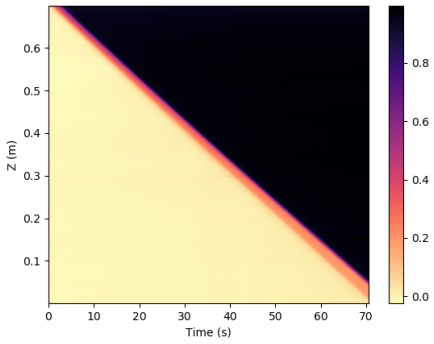

(a) v = 12 mm/s

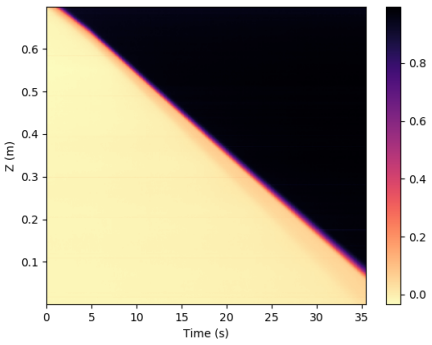

(b) v = 25 mm/s

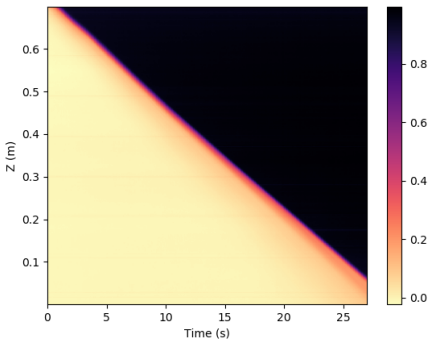

(c) v = 33 mm/s

FIGURE 4.6: Spatiotemporal diagrams for stable-density with At = 0.02

(a) v = 12 mm/s

(b) v = 25 mm/s

(c) v = 33 mm/s

FIGURE 4.7: Fluid displacement for stable-density with At = 0.02

At = 0, iso-dense

In this section, the effect of the flow velocity in iso-dense displacement is studied. Figure 4.8 shows spatiotemporal diagrams for Atwood number of zero at different flow velocities. Transverse and backflow are not observed during the displacement since the density is the same for the displacing and the displaced fluid. The flow displacement is uniform during the experiments. Moreover, it is clear that increasing the imposed velocity results in shorter displacement time and higher front velocity.

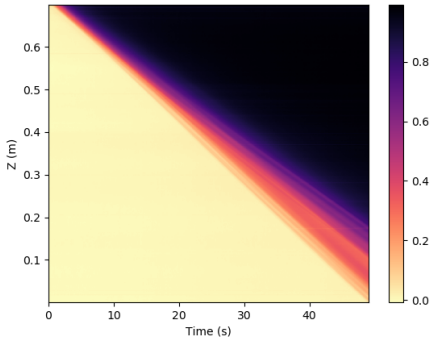

(a) v = 12 mm/s

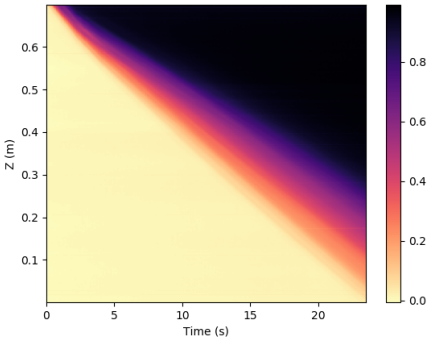

(b) v = 25 mm/s

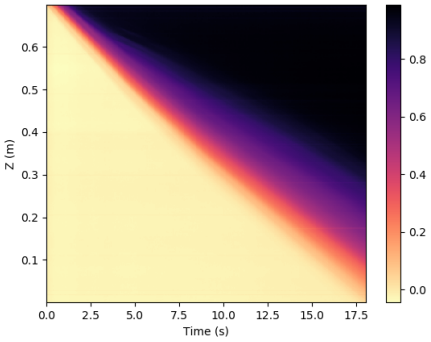

(c) v = 33 mm/s

FIGURE 4.8: Spatiotemporal diagrams for At = 0

As an example, Figure 4.9 shows the fluid displacement for v = 25 mm/s at different time intervals from the front, the right side, and the left side of the annulus in the mirrors. In this Figure, it can be seen there is a less clear interface in comparison with the previous case, Figure 4.7. The front of heavy fluid has reached the bottom faster compared to the case with denser displaced fluid.

(a) The right side of the annulus in the mirror

(b) The front side of the annulus

(c) The left side of the annulus in the mirror

FIGURE 4.9: Fluid displacement for At = 0 and v = 25 mm/s

4.4.2 Unstable-density displacement

In unstable-density displacement, heavy fluid is placed above the lighter fluid. The effect of the flow velocity has been studied for Atwood numbers of 0.003 and 0.02. Figure 4.10 and Figure 4.11 demonstrate the effect of imposed velocity on the velocity of the front and fluid displacement time quantitatively. In general, displacement time is proportional to the inverse of front velocity. Increasing the imposed velocity results in higher front velocity and shorter time of displacement.

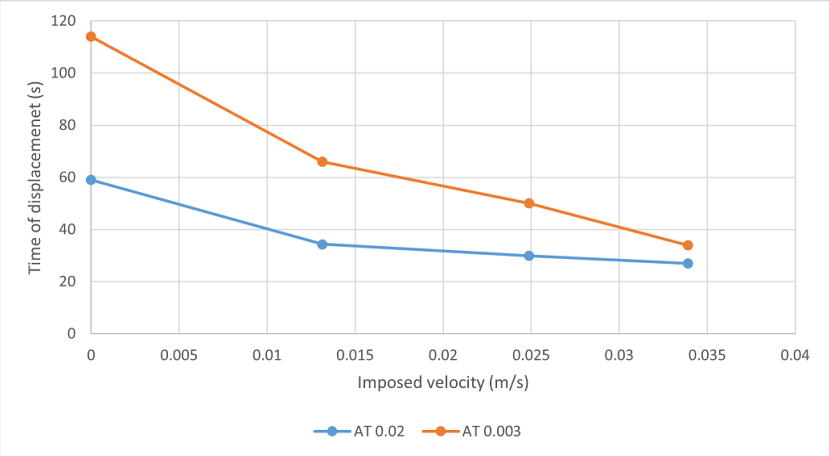

FIGURE 4.10: Time of displacement versus imposed velocity for different Atwood numbers

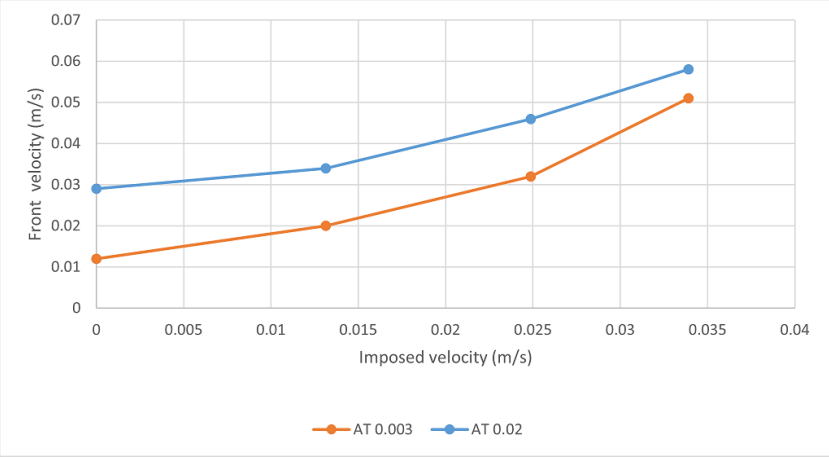

FIGURE 4.11: Front velocity versus imposed velocity for different Atwood numbers

Figure 4.12 shows spatiotemporal diagrams for At = 0.02 at different flow velocities. Although there is a higher front velocity at a higher imposed velocity, the upward movement of light fluid decreases by increasing the imposed velocity, and backflow becomes suppressed, leading to more efficient displacement. As an example, Figure 4.13 shows the fluid displacement from the front side of the annulus for At = 0.02 and four fluid velocities at different time intervals.

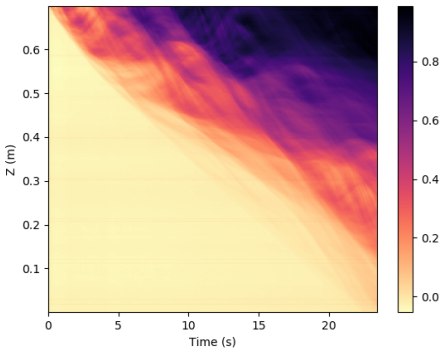

(a) No flow

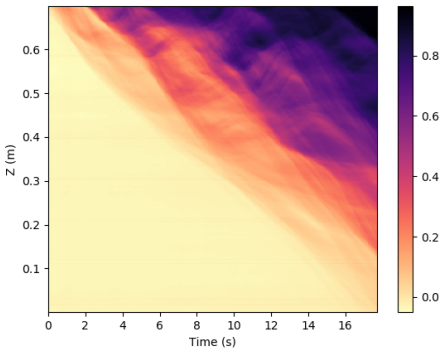

(b) v = 12 mm/s

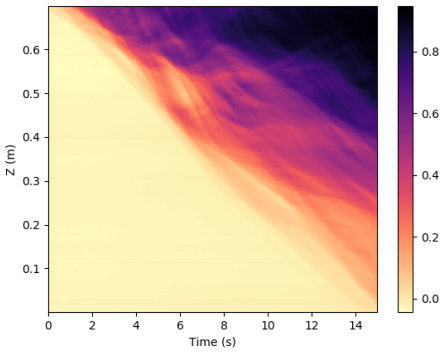

(c) v = 25 mm/s

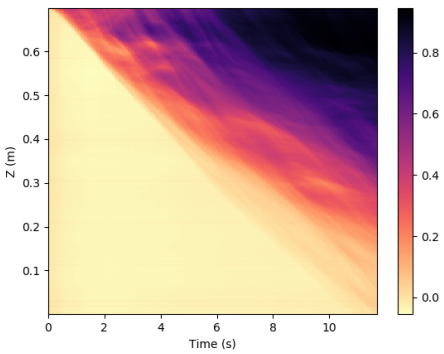

(d) v = 33 mm/s

FIGURE 4.12: Spatiotemporal diagrams for At = 0.02

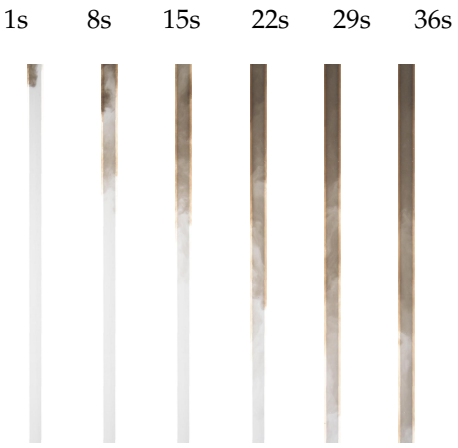

(a) No flow

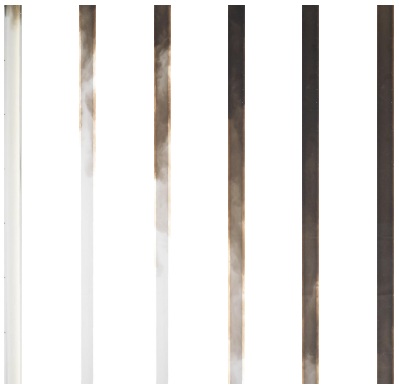

(b) v = 12 mm/s

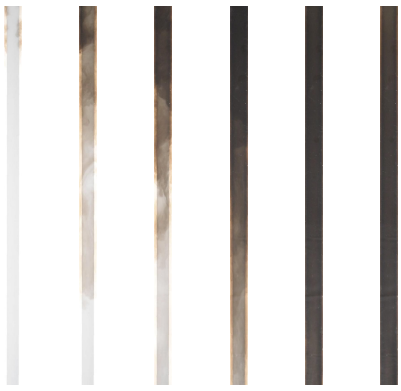

(c) v = 25 mm/s

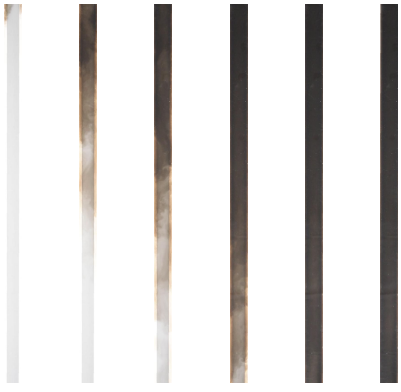

(b) v = 33 mm/s

FIGURE 4.13: Fluid displacement for At = 0.02

4.5 Effect of Atwood number

The effect of the density difference between displaced and displacing fluid is investigated in this section. The fluid velocity is kept constant while the Atwood number is altered for each run.

4.5.1 Exchange flow

For these cases, the imposed velocity is zero, and the fluid displacement is just due to gravitational force and buoyancy. There is only exchange flow, and the displacement is dominated by Rayleigh-Taylor instability due to density difference. As shown in Figure 4.14, the mixing zone grows faster for Atwood number of 0.02 than 0.003. Regarding studying the flow pattern, stronger backflow is seen for the higher Atwood numbers.

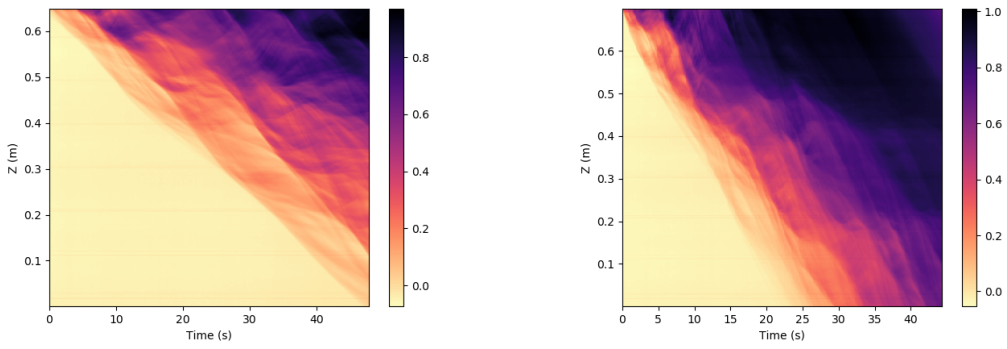

(a) At = 0.003 (b) At = 0.02

FIGURE 4.14: Spatiotemporal diagrams for v = 0

4.5.2 Imposed velocity

Figure 4.15 to Figure 4.17 compare the spatiotemporal diagrams of different displacements with different density ratio at different range of velocities. What is clear in all of these figures is that there is more mixing between two fluids with increasing density instability. Sections (a) and (b) in these figures show the result of stable displacement, and two others are from the heavy over light fluid displacement. For two stable cases, there are no instabilities, and a thin stable mixing zone exists for isodense cases (section (b) in the mentioned figures). Regarding unstable cases (sections (c) and (d)), there is a stronger backflow at higher density ratios, while with increasing the imposed velocity, the effect of the Atwood number decrease.

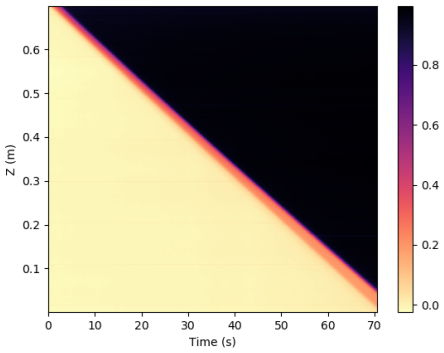

(a) At = 0.02

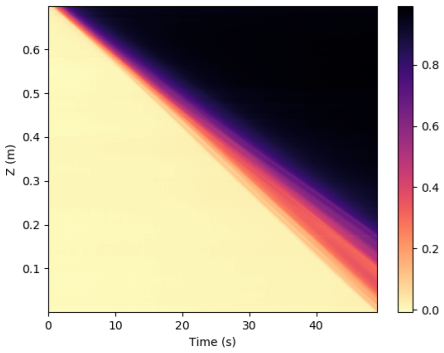

(b) At = 0

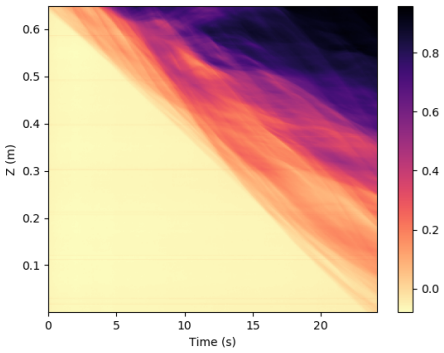

(c) At = 0.003

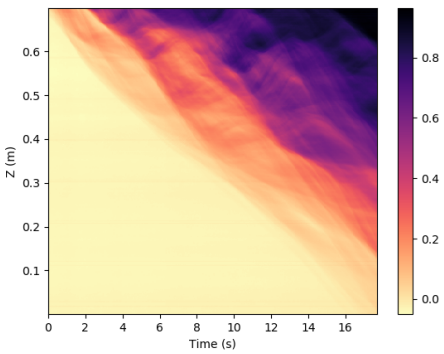

(d) At = 0.02

FIGURE 4.15: Spatiotemporal diagrams for v = 12 mm/s.
(a) stable-density, (b) iso-dense, (c) unstable-density, (d) unstable-density

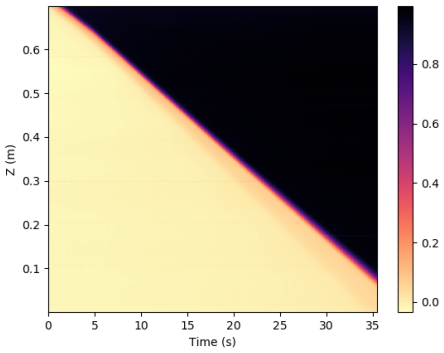

(a) At = 0.02

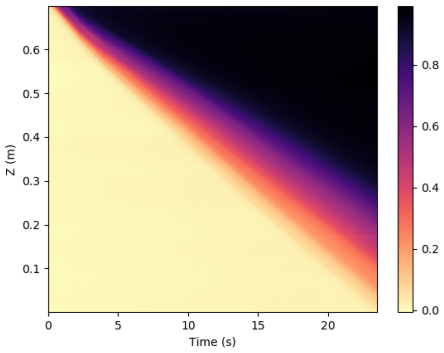

(b) At = 0

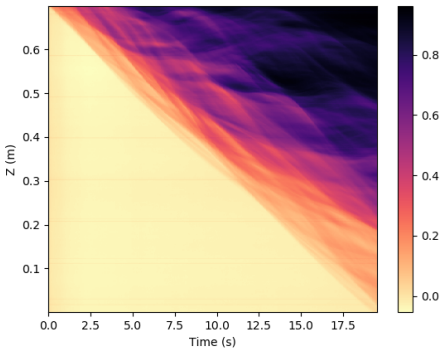

At = 0.003

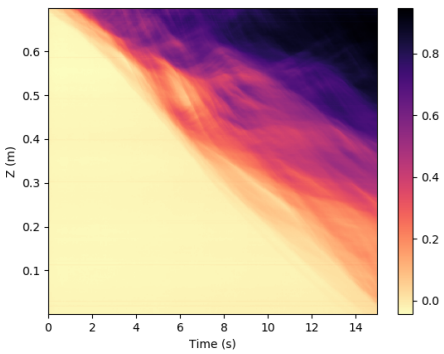

(d) At = 0.02

FIGURE 4.16: Spatiotemporal diagrams for v = 25 mm/s.
(a) stable-density, (b) iso-dense, (c) unstable-density, (d) unstable-density

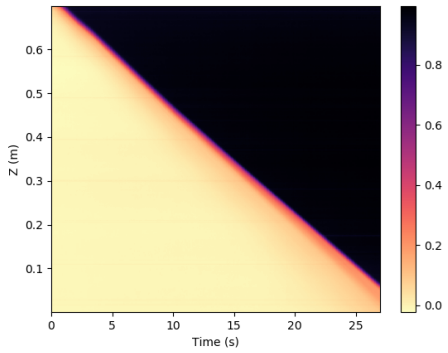

(a) At = 0.02

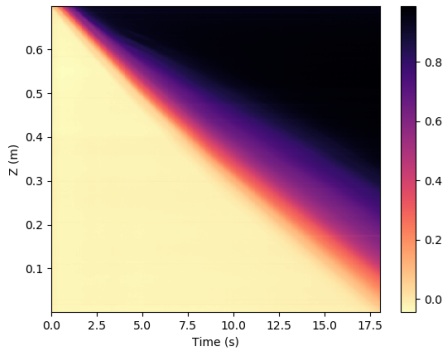

(b) At = 0

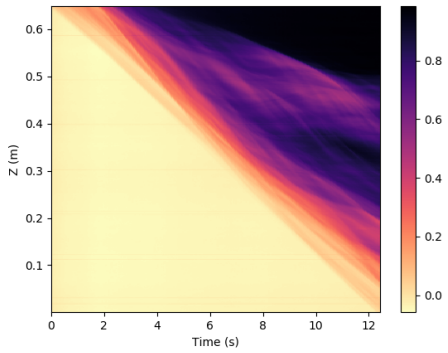

(c) At = 0.003

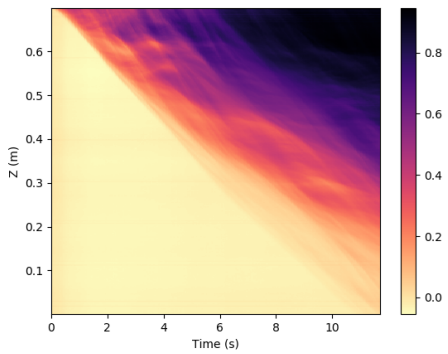

(d) At = 0.02

FIGURE 4.17: Spatiotemporal diagrams for v = 33 mm/s.
(a) stable-density, (b) iso-dense, (c) unstable-density, (d) unstable-density

The weaker effect of the Atwood number at higher imposed velocity can be seen in Figure 4.18. In this Figure, the front velocity versus Atwood number at different ranges of imposed velocity is plotted.

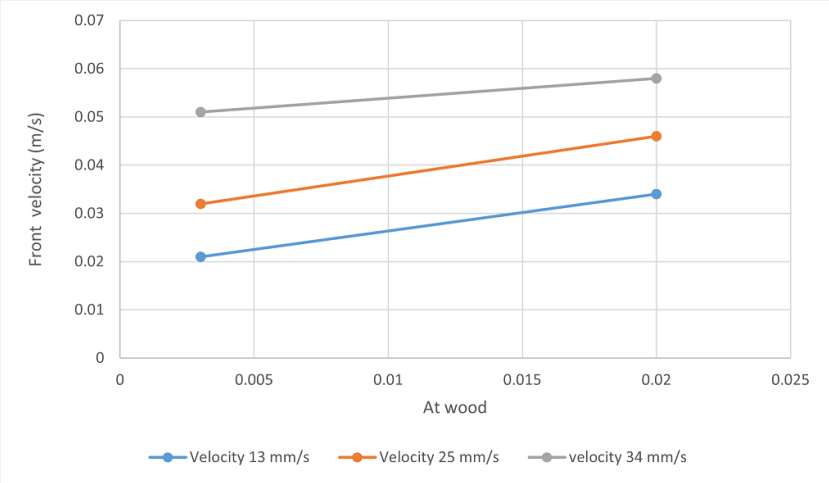

FIGURE 4.18: Front velocity versus Atwood number for different imposed velocities

Chapter 5

Conclusion

In this thesis, the displacement flow of two Newtonian, miscible fluids with a density ratio in a vertical, concentric annulus related to the cementing operation in oil and gas wells has been studied experimentally. For this purpose, a transparent annulus flow loop has been designed and constructed. A series of experiments have been done for stable and unstable-density displacement; however, the main focus of this study is heavy over light and unstable-density displacement. The effect of imposed velocity and density ratio on fluid displacement are investigated.

The results show that flow velocity and density differences affect flow patterns and fluid instabilities. In unstable-density cases, Rayleigh-Taylor instability leads to backflow and transverse flow. By increasing the Atwood number, there is a higher tendency to backflow and transverse flow, and the mixing zone grows faster. A shorter time of displacement is observed for cases with heavier displacing fluid. On the other hand, increasing the imposed velocity can suppress the backflow and weaken the effect of the Atwood number. It is evident that a higher imposed velocity shortens the time of the displacement and increases the front velocity of the mixing zone.

As mentioned earlier, a series of stable-density displacement experiments have been done to compare with unstable ones. For these cases, the light fluid displaces the heavy fluid, and the Atwood number of zero (iso-dense fluids) and 0.02 are considered. There is not any backflow or transverse flow. A sharp, steady interface separates the displacing and displaced fluids during fluid displacement. Although this interface is less clear for iso-dense displacement than the Atwood number of 0.02, the flow displacement is still uniform. Also, the front of displacing fluid goes faster when the fluids are iso-dens in comparison with the case with denser displaced fluid. The higher imposed velocity leads to a shorter time of displacement and higher front velocity in both cases.

The significant effect of imposed velocity and fluid density difference has been shown. Higher front velocity and shorter displacement time are obtained by increasing the Atwood number. However, it should be mentioned that the higher front velocity or shorter displacement time might not necessarily result in a more effective cementing

job since there is a stronger backflow and a thicker mixing zone at a higher Atwood number. It seems that by imposing a higher velocity, the backflow and mixing zone can be shrunk, and the efficiency of cementing operation is increased.

5.1 Recommendation for future work

Newtonian, miscible fluid with low viscosity has been investigated in this study, while the fluid can be non-Newtonian and immiscible, with higher viscosity in the oil and gas industry. Investigation of displacement flow of high viscous and immiscible (Newtonian and non-Newtonian) fluid is helpful in cementing jobs. As in practice, oil and gas wells can be eccentric and inclined; studying the effect of these two parameters, which strongly affect fluid displacement, is recommended for further studies.

5.1.1 Improvement of the experimental setup

- Changing the type of the outlet valve to be able to control the flow velocity easier.
- Upgrading the setup by adding a function to vibrate or rotate the inner pipe to study the effect of tubing movement on fluid displacement.
- Changing the pressure sensor with a higher resolution one that is capable of sensing the pressure difference due to the density difference of the fluids.

References

[1] MHI Baird et al. "Unsteady axial mixing by natural convection in a vertical column". In: *AIChE journal* 38.11 (1992), pp. 1825–1834.

[2] Erik B Nelson. "Well Cementing, 2nd Edition,Schlumberger Educational Service". In: *Sugar Land, Texas 77478* (2006).

[3] E Kuru and S Seatter. "Reverse circulation placement technique vs. conventional placement technique: A comparative study of cement job hydraulics design". In: *Journal of Canadian Petroleum Technology* 44.07 (2005), pp. 16–19.

[4] S Pelipenko and IA Frigaard. "Visco-plastic fluid displacements in near-vertical narrow eccentric annuli: prediction of travelling-wave solutions and interfacial instability". In: *Journal of Fluid Mechanics* 520 (2004), pp. 343–377.

[5] T Séon et al. "Buoyancy driven miscible front dynamics in tilted tubes". In: *Physics of fluids* 17.3 (2005), p. 031702.

[6] Ali Etrati, Kamran Alba, and Ian A Frigaard. "Two-layer displacement flow of miscible fluids with viscosity ratio: Experiments". In: *Physics of Fluids* 30.5 (2018), p. 052103.

[7] S Malekmohammadi et al. "An experimental study of laminar displacement flows in narrow vertical eccentric annuli". In: *Journal of fluid mechanics* 649 (2010), pp. 371–398.

[8] Hanieh K Foroushan et al. "Cement Placement: An Overview of Fluid Displacement Techniques and Modelling". In: *Energies* 14.3 (2021), p. 573.

[9] Rafael Hernandez and Daniel Bour. "Reverse-Circulation Method and Durable Cements Provide Effective Well Construction: A Proven Technology". In: *Thirty-Fifth Workshop on Geothermal Reservoir Engineering*. 2010.

[10] Doug MacEachern et al. "Reverse Foam Cementing an Offshore Production Tieback". In: *Oral presentation of paper AADE-03-NTCE-32 given at the AADE*

2003 National Technology Conference—Practical Solutions for Drilling Challenges, Houston. 2003, pp. 1–3.

[11] Tim Marriott et al. "Reverse-Circulation Cementing To Seal a Tight Liner Lap". In: *Offshore Technology Conference*. OnePetro. 2007.

[12] R Balasubramaniam et al. "Instability of miscible interfaces in a cylindrical tube". In: *Physics of Fluids* 17.5 (2005), p. 052103.

[13] Jun Kuang, P Petitjeans, and T Maxworthy. "Velocity fields and streamline patterns of miscible displacements in cylindrical tubes". In: *Experiments in fluids* 37.2 (2004), pp. 301–308.

[14] J Scoffoni, E Lajeunesse, and GM Homsy. "Interface instabilities during displacements of two miscible fluids in a vertical pipe". In: *Physics of Fluids* 13.3 (2001), pp. 553–556.

[15] Marie Debacq et al. "Self-similar concentration profiles in buoyant mixing of miscible fluids in a vertical tube". In: *Physics of fluids* 13.11 (2001), pp. 3097–3100.

[16] K Alba, SM Taghavi, and IA Frigaard. "Miscible density-unstable displacement flows in inclined tube". In: *Physics of Fluids* 25.6 (2013), p. 067101.

[17] Ali Etrati and Ian Frigaard. "Laminar Displacement Flows in Vertical Eccentric Annuli: Experiments and Simulations". In: *International Conference on Offshore Mechanics and Arctic Engineering*. Vol. 58875. American Society of Mechanical Engineers. 2019, V008T11A062.

[18] *Drilling Course,Introduction to Casing*. `[Online] .Available : https : / / www . drillingcourse . com / 2015 / 12 / introduction - to - casing . html`. 2015, (accessed: 23.01.2022).

[19] Martijn Bogaerts et al. "Reverse Cement Placement Technique: A Case Study from Deepwater Gulf of Mexico". In: *SPE Deepwater Drilling and Completions Conference*. OnePetro. 2014.

[20] *Schlumberger, Deviation*. `[Online] .Available : https : / / glossary . oilfield . slb . com/Terms/d/deviation . aspx`. (accessed: 04.03.2022).

[21] Mahmoud Khalifeh and Arild Saasen. "Fundamentals of plug placement". In: *Introduction to Permanent Plug and Abandonment of Wells*. Springer, 2020, pp. 185–212.

[22] *Schlumberger, Eccentric*. [Online] . Available : https : //glossary . oilfield . slb . com/en/terms/e/eccentric. (accessed: 23.01.2022).

[23] *X-engineer,What is fluid density*. [Online] . Available : https : //x - engineer . org/fluid-density/. (accessed: 23.01.2022).

[24] Anne Helmenstine. *Viscosity Definition and Examples*. [Online] . Available : https://sciencenotes.org/viscosity-definition-and-examples/. November 18, 2021, (accessed: 23.01.2022).

[25] *ScienceDirect,Reynolds number*. [Online] . Available:https://www.sciencedirect. com/topics/engineering/reynolds-number. (accessed: 23.01.2022).

[26] David L Youngs. "Three-dimensional numerical simulation of turbulent mixing by Rayleigh–Taylor instability". In: *Physics of Fluids A: Fluid Dynamics* 3.5 (1991), pp. 1312–1320.

[27] *Froude Number and Flow States*. [Online] . Available : http : //www . fsl . orst . edu/geowater/FX3/help/8_Hydraulic_Reference/Froude_Number_and_Flow_ States . htm. (accessed: 23.01.2022).

[28] Sardar Malekmohammadi. "An experimental study of two multi-fluid flows of interest to the oilfield cementing industry". PhD thesis. University of British Columbia, 2009.

[29] *Ansys,Kelvin-Helmholtz Instability Between Two Fluids*. [Online] . Available:https: //courses . ansys . com/index . php/courses/basics - of - turbulent - flows/ lessons/simulation-exampleshomework-quizzes/topic/kelvin-helmholtz- instability-between-two-fluids-simulation-example/. (accessed: 23.01.2022).

[30] Jin Matsumoto, Miguel A Aloy, and Manel Perucho. "Linear theory of the Rayleigh–Taylor instability at a discontinuous surface of a relativistic flow". In: *Monthly Notices of the Royal Astronomical Society* 472.2 (2017), pp. 1421–1431.

[31] P Ramaprabhu and MJ Andrews. "Experimental investigation of Rayleigh–Taylor mixing at small Atwood numbers". In: *Journal of Fluid Mechanics* 502 (2004), pp. 233–271.

[32] John D Anderson. "Governing equations of fluid dynamics". In: *Computational fluid dynamics*. Springer, 1992, pp. 15–51.

[33] *COMSOL, Navier-stokes equation*. [Online] . Available : https : //www . comsol . com/multiphysics/navier-stokes-equations. 2015 (accessed: 08.02.2022).

[34] H. J. Skadsem. "personal communication". In: May 2021.

[35] Sjur Haugen Bjørlo. "An Experimental Study of "Heavy over Light" Density-Unstable Displacement of Newtonian Fluids in a Vertical Annular Geometry of Interest to Reverse Circulation Cementing. M.S. thesis, Department of petroleum Engineering, Stavanger". In: 2021.

[36] Annegret Hans and Bernhard Hochstein. "In-line viscometry by using a modified electromagnetic flowmeter". In: *Proceedings of the 6th European Conference on Rheology (Eurheo), Erlangen, S*. Citeseer. 2002, pp. 483–484.

[37] PAAR ANTON. "Instruction Manual: DMA 4100 M, DMA 4500 M, DMA 5000M". In: *Austria: Anton Paar* (2012).

[38] Inc OFI Testing Equipment. "Instruction Manual: Model 800 Viscometer". In: *Texas. U.S.A* (2016).

[39] *DRAWING INK FROM KOH-I-NOOR*. `[Online] .Available : https : / / www . kunstnerutstyr.no/blekk.html`. (accessed: 09.06.2022).

Appendices

Appendix A

Calibration

A.1 Flowmeter

To calibrate the flowmeter, first, the setup is filled with water, and the pump is started. The pump is set to 7.8 v and 3.2 A for all cases. Then, the voltage of the flowmeter is set at a constant value by adjusting the outlet valve, and the process is continued for different voltages and valve openings. The required time to fill a 2000 mL Erlenmeyer flask placed at the outlet valve is recorded to measure the flowrate. Table A.1 illustrates the tests with different voltages and velocities.

TABLE A.1: Flowmeter calibration

Voltage(v)	Time	Q(ml/s)	v(mm/s)	Re
1.18	4′57″	6.7	8.7	132
1.33	1′56″	17.2	22.5	338
1.42	1′24″	23.8	31.1	466
1.53	1′02″	32.2	42.1	632
1.62	52″	38.4	50.2	753
1.73	44″	45.4	59.3	890
1.85	38″	52.6	68.7	1031
1.95	33″	60.6	79.1	1187
2.15	27″	74.1	96.7	1451

As shown below, by using the mass balance between inlet and outlet, It is seen that the inlet velocity is related to the fluid's density. The light fluid is freshwater, and the density is considered constant, but with changing heavy fluid's density, inlet velocity is changed.

$$m_{inlet} = m_{outlet} \tag{A.1}$$

$$\rho_H.Q_H = \rho_L.Q_L \tag{A.2}$$

$$Q_H = \frac{\rho_L}{\rho_H}.Q_L \quad \text{and} \quad \alpha = \frac{\rho_L}{\rho_H} \tag{A.3}$$

$$V_H = \alpha.\frac{Q_L}{A_{annulus}} \tag{A.4}$$

The density of the heavy fluid is not too high in the experiments, so α is close to 1, which can be neglectable.
Figure A.1 shows the linear correlation between velocity and voltage used to calculate the velocity in the experiments. Equation A.5 presents the best fit line from plotting the velocity versus voltage.

$$y = 90.237x - 97.078 \tag{A.5}$$

Where:

y = fluid velocity (mm/s)
x = voltage (v)

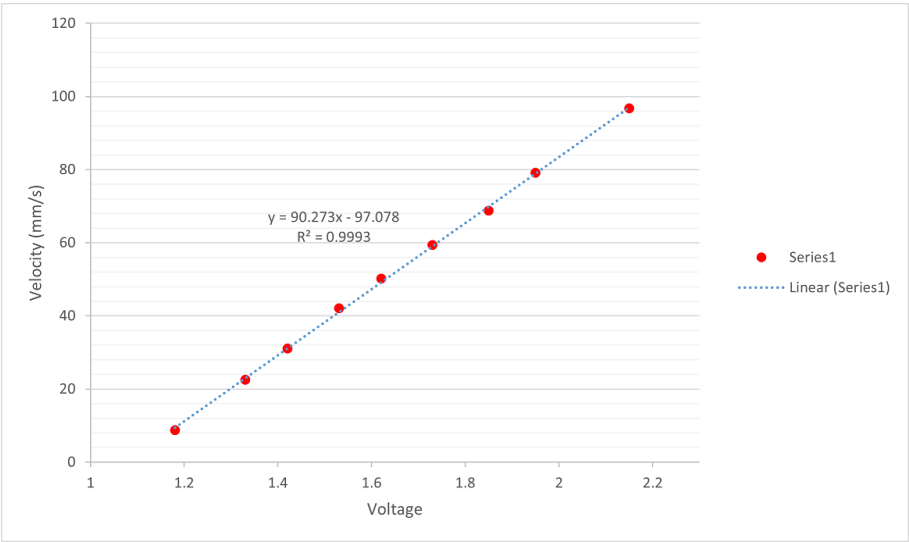

FIGURE A.1: Correlation of the velocity and voltage

A.2 Pressure sensor

The pipe is filled with water to a specific height from the pressure sensor, and pressure is recorded in the Pasco system. The height of the water is changed to a lower level in each step, and hydrostatic pressure is measured. Figure A.2 shows pressure versus time for different heights of the water.

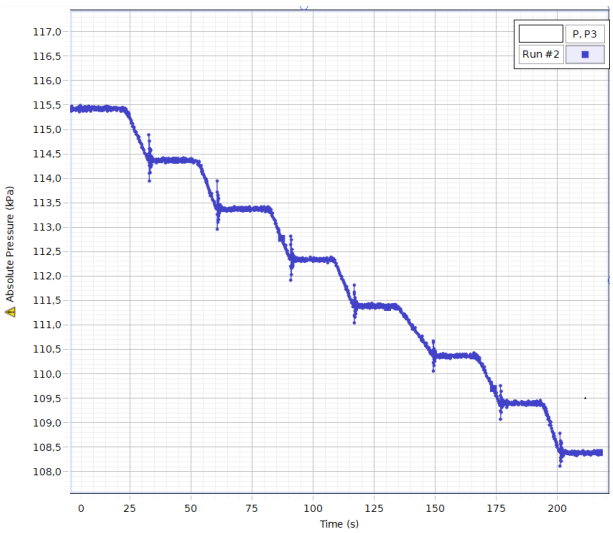

FIGURE A.2: Pressure test

Also, the theoretical hydrostatic absolute pressure is calculated by the equation A.6:

$$P = \rho g h + 101300 \tag{A.6}$$

Tables A.2 shows the result of experimental and theoretical pressure for different heights.

TABLE A.2: Result of the experimental and theoretical pressure

Height (m)	**Experimental pressure (kpa)**	**Theoretical pressure (kpa)**
0.695	108.4	108.1
0.8	109.4	109.1
0.898	110.3	110.1
1	111.3	111.1
1.098	112.3	112
1.2	113.3	113
1.3	114.3	114
1.405	115.4	115

Figure A.3 shows the experimental pressure recorded by the PASCO system and the theoretical pressure versus height. It is seen that there are good matches between the two graphs, and the calibration of the pressure sensor is acceptable.

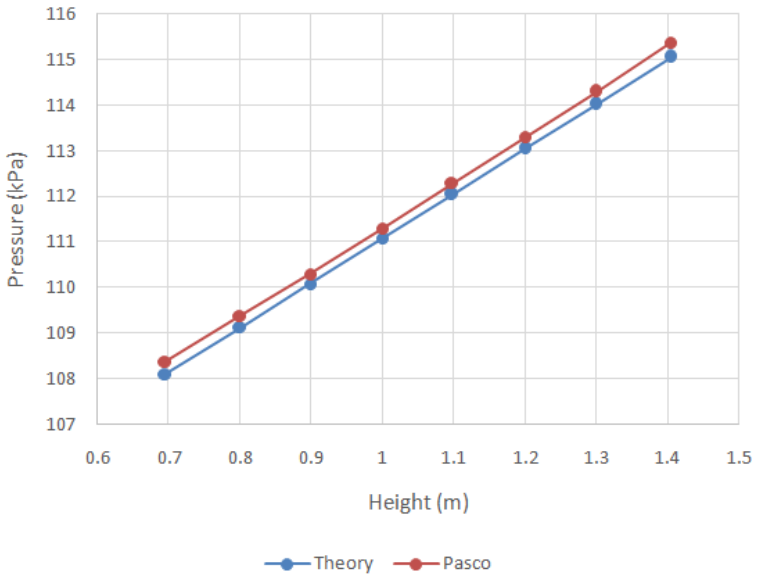

FIGURE A.3: Experimental pressure against theoretical pressure

Appendix B

Fluid Preparation

B.1 Density of the heavy fluid

As mentioned before, salt is used to increase the density of the heavy fluid. Table B.1 shows the amount of salt added to water to get a specific density for the different experimental runs. The density is measured by a density meter.

TABLE B.1: Heavy fluid density with different concentrations of the salt

Solution	**Temperature** ($^{\circ}C$)	**Density** ($\frac{kg}{m^3}$)	**Atwood Number**
Pure water	20	0.998	-
100 ml water + 1 gr salt (NaCl)	20	1.005	0.003
100 ml water + 6 gr salt (NaCl)	20	1.038	0.02

B.2 Visibility of the heavy fluid

A visibility test was done to find the best solution for heavy fluid to see the details of the flow displacement. First, 15 ml of ink is added to 1000 ml of displacing fluid. As shown in the Figure B.1a, the solution is too light, and it is challenging to investigate the details of the flow. However, by increasing the amount of the ink to 30 ml per 1000 ml of heavy fluid, the visibility of the displacement is improved (see Figure B.1b). Figure B.2 shows the drawing ink used in this experiment which is soluble in water [39].

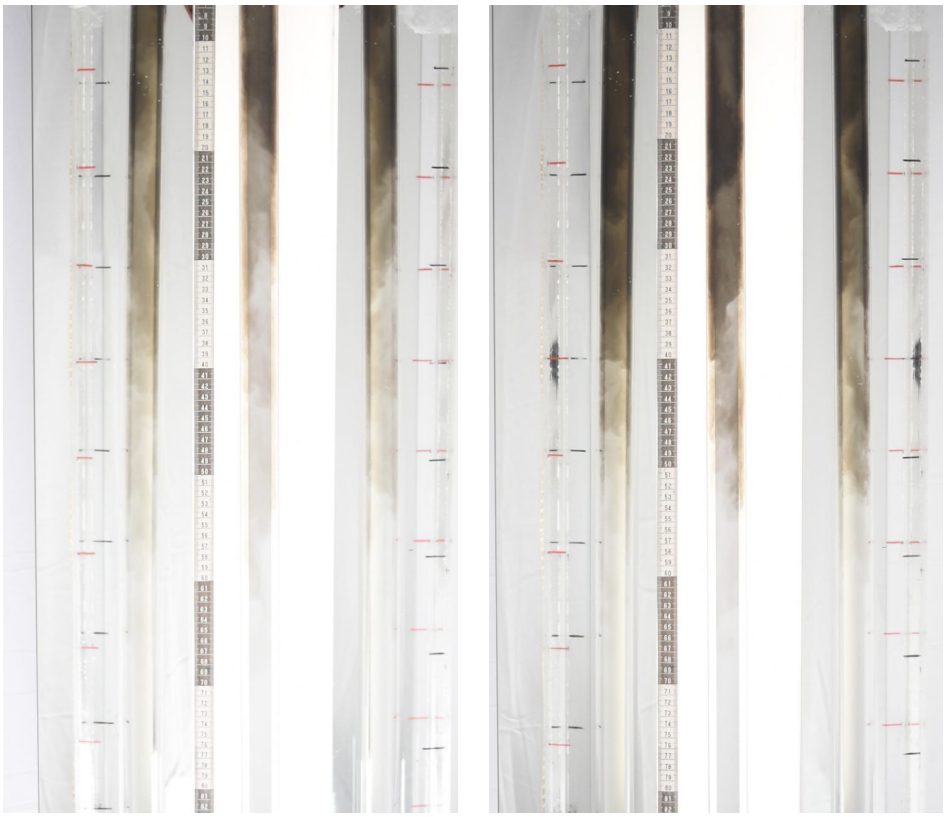

(a) (b)

FIGURE B.1: Visibility test.
(a) 15 ml ink in 1000 ml displacing fluid, (b) 30 ml ink in 1000 ml displacing fluid

FIGURE B.2: Ink

Appendix C

Images of the experimental setup

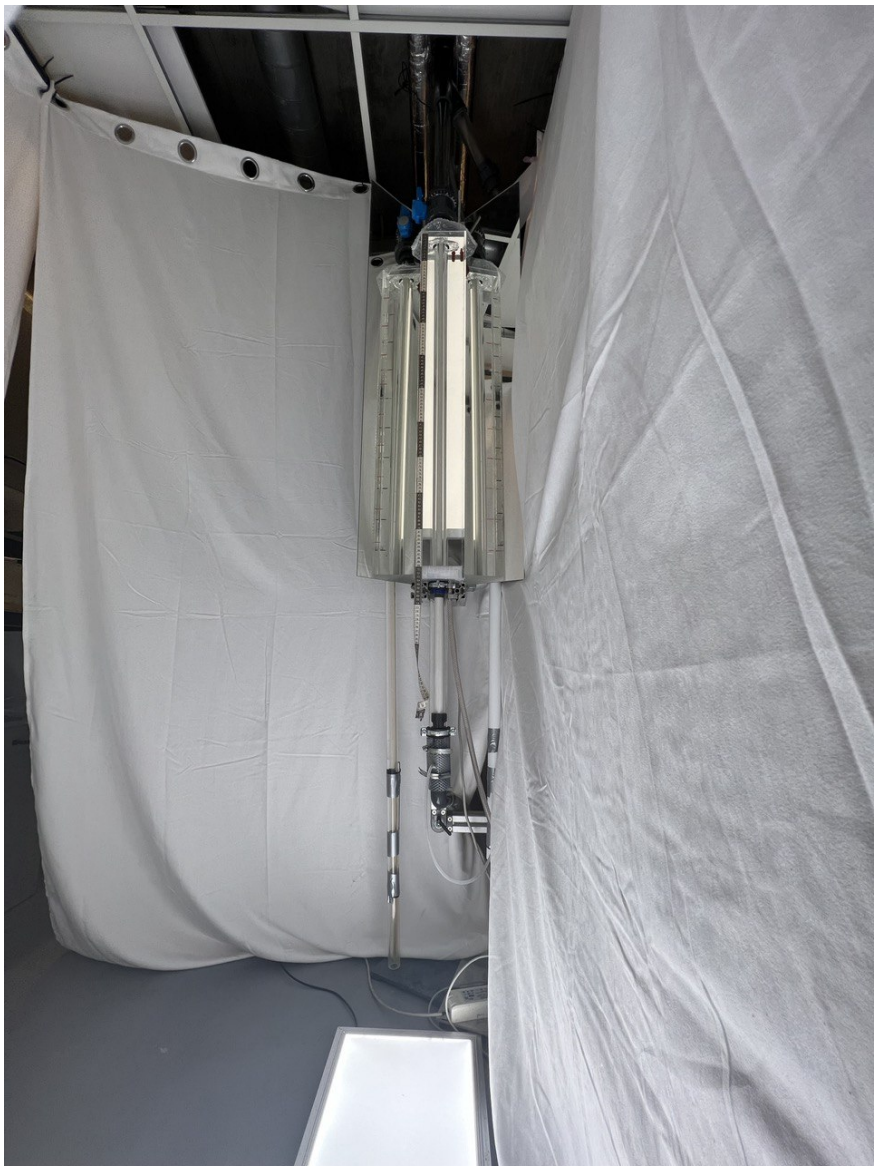

FIGURE C.1: The experimental setup

FIGURE C.2: Ball valve used to separate the heavy and light fluid

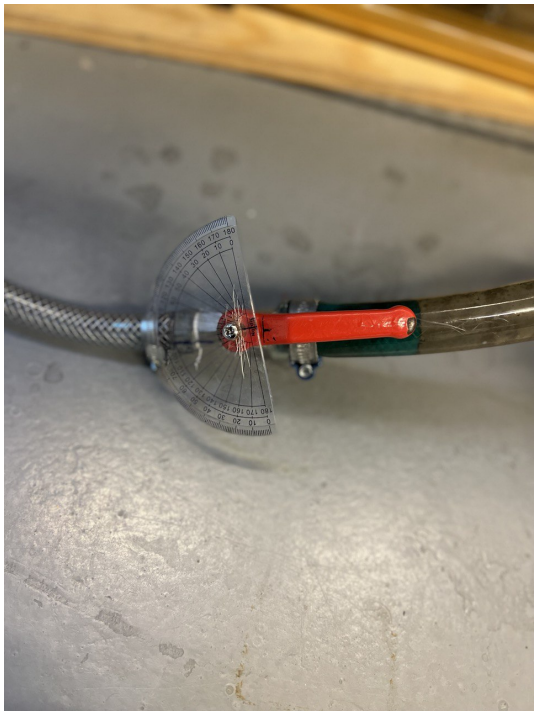

FIGURE C.3: Outlet valve

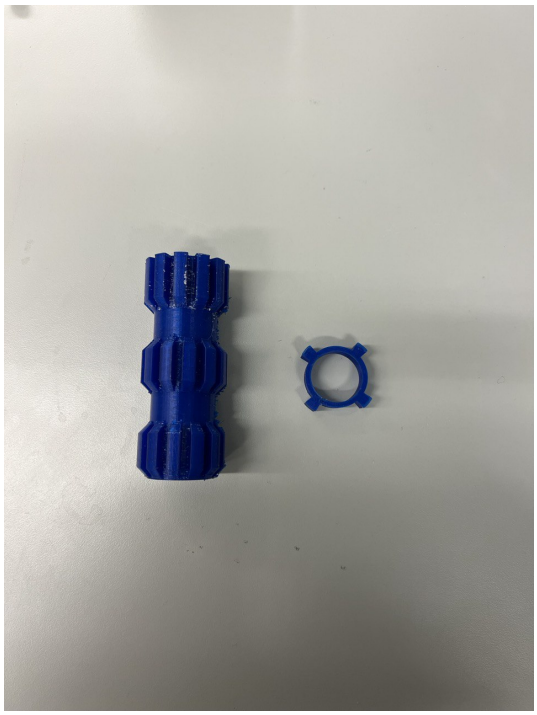

FIGURE C.4: Eccentricity control and flow straightener

FIGURE C.5: Lever to control the inclination

FIGURE C.6: Y-coupling

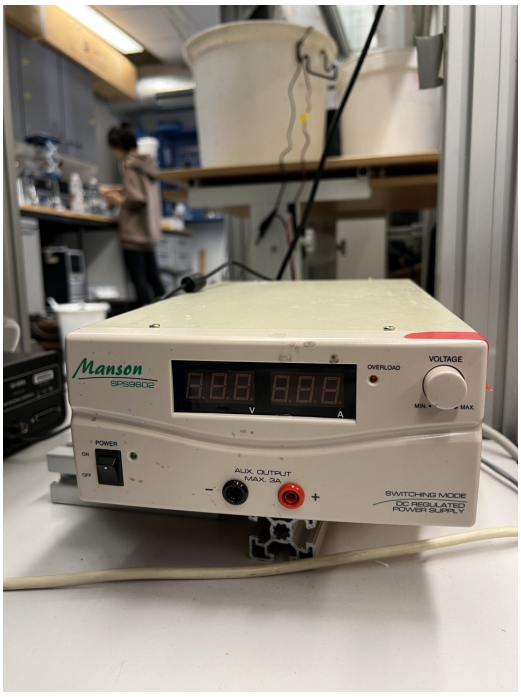

FIGURE C.7: Heavy fluid reservoir, pump and power supply

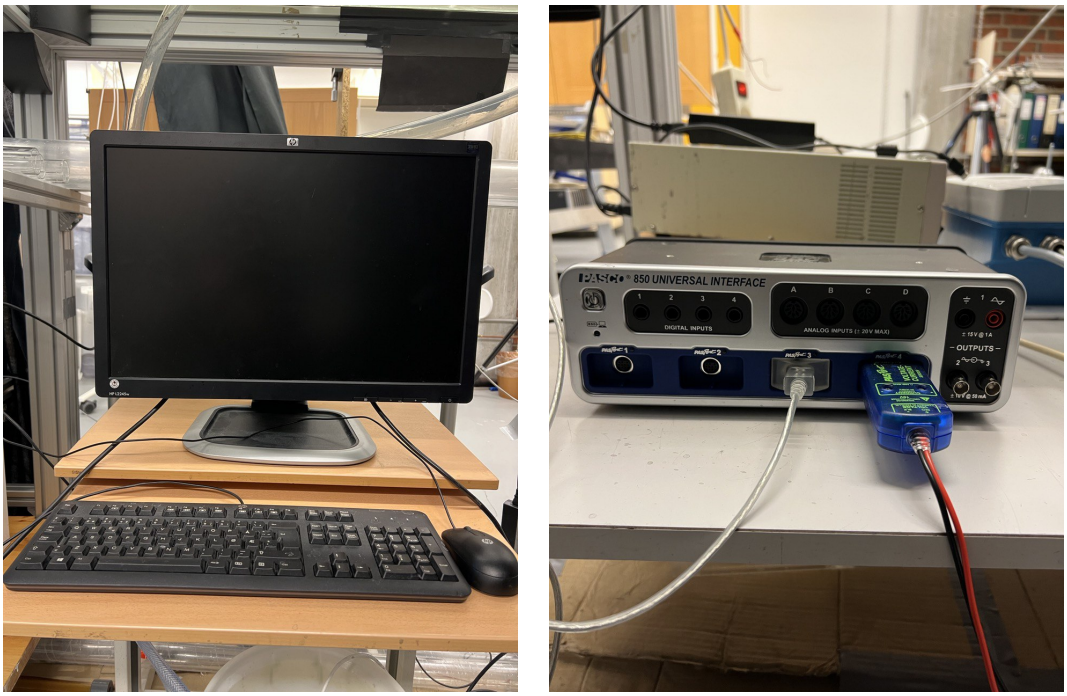

FIGURE C.8: Computer and PASCO system

FIGURE C.9: Camera system, curtains and light

FIGURE C.10: Pressure sensor and connecting tubes

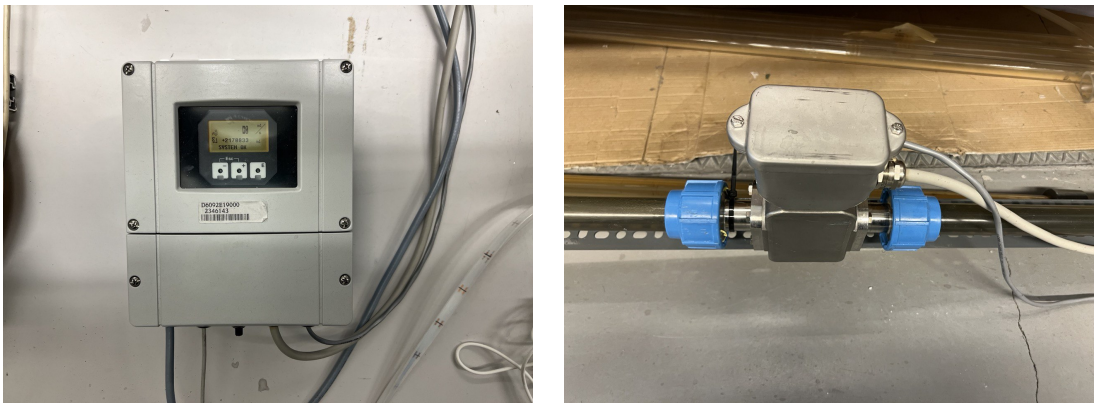

FIGURE C.11: Flowmeter and flowmeter display

FIGURE C.12: Density meter

Appendix D

Observations

- The inclination of the pipe was changed, and some experimental runs were performed to prove that the pipe can be inclined perfectly. The pipe angle was changed from the vertical direction to 10 degrees, and flow displacement was recorded at different time intervals. The Figure D.1 confirms that the fluid displacement is logical, and the effect of the inclination can be analyzed by this experimental setup.

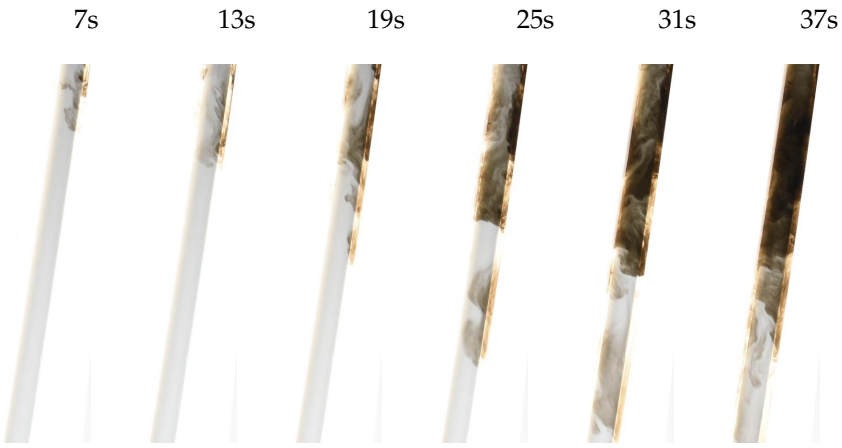

FIGURE D.1: Example of fluid displacement for inclined situation

- As Figure D.2 shows a container with a bilge pump, and its connections for fluid with higher viscosity are prepared. Some experiments were performed and confirmed that the equipment works perfectly. Glycerol was used to increase the fluid viscosity, and viscosity was measured by a viscometer. Also, the density of Glycerol is 1.26 $gr/cm3$, which can affect the density of the fluid.

FIGURE D.2: Container and pump for viscous solution, and glycerol

- For eccentricity control, some connectors were designed for the top and bottom of the pipe with different shapes and lengths, as shown in Figure D.3. However, It was challenging to set the pipes concentric. Another thin connector was added to the middle of the pipe below the fish tank to solve this problem.

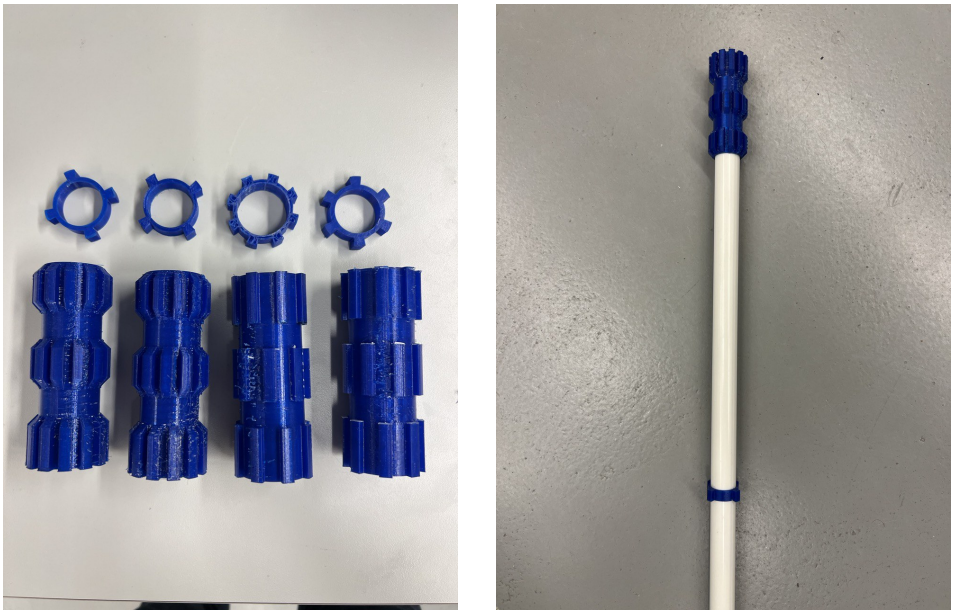

FIGURE D.3: Connectors and flow straightener

- At the beginning of the experiment, a metal pipe with a 30 mm outer diameter was used as the inner pipe. The pipe was painted by hand in white. There were some problems with the rigidity of the pipe. Also, the color was removed during the experiments. Finally, the problem was solved by changing the pipe with

a multilayer composite pipe with a 25 mm outer diameter which was painted by the factory (see Figure D.4).

FIGURE D.4: Changing the inner pipe

- At first, the length of the pipe up to the ball valve was 2 meters, and it was close to the floor. The hose that connected the end of the annulus to the outlet was laid down horizontally on the floor. It was difficult to discharge the fluid entirely and wash the setup perfectly. For this reason, the pipe was cut by around half a meter to solve the problem (see Figure D.5).

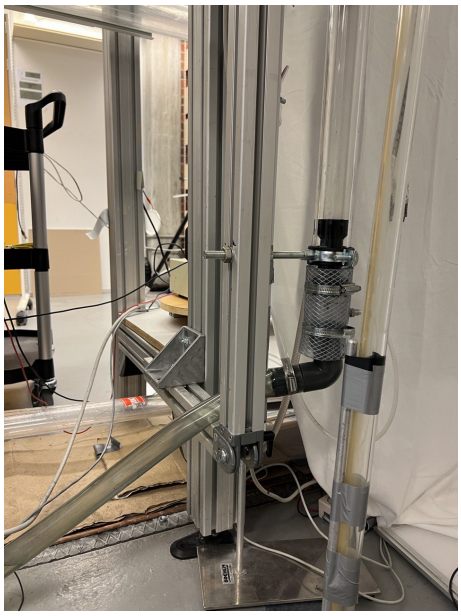

FIGURE D.5: Cutting the pipes

- Curtains were placed around the setup to improve the natural background and upgrade the visualization. First, black curtains were selected. After some experiments, reflection was observed in videos. So, black curtains were replaced by white curtains to remove the reflection (see Figure D.6).

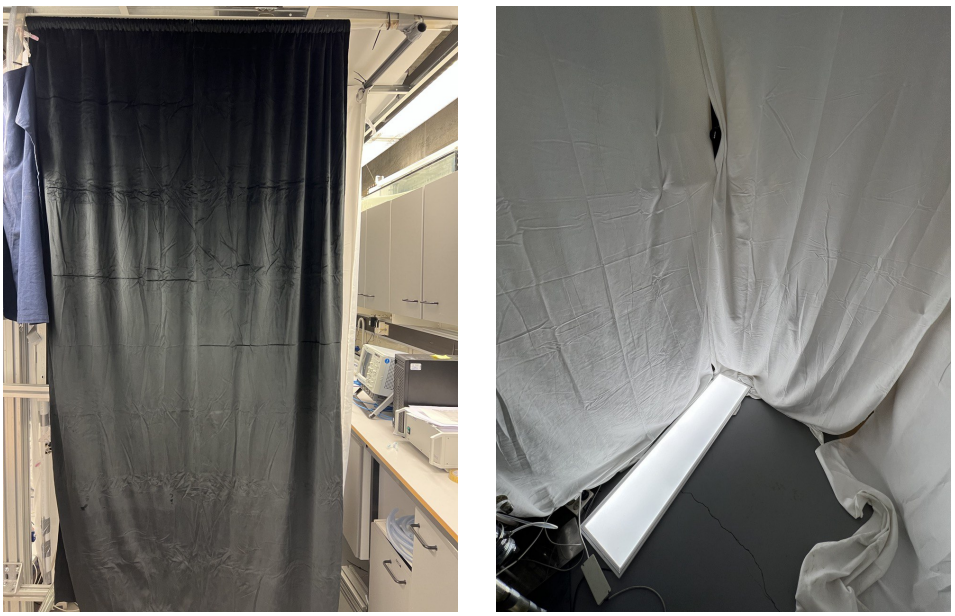

FIGURE D.6: Changing the curtains

- There was a problem with supplying the heavy fluid from the heavy fluid container to the top of the setup. To solve this problem, the old pump with a capacity of 63 l/min (12 v and 5 A) was changed with a more powerful one with a 95 l/min capacity (12 v and 8 A) (see Figure D.7).

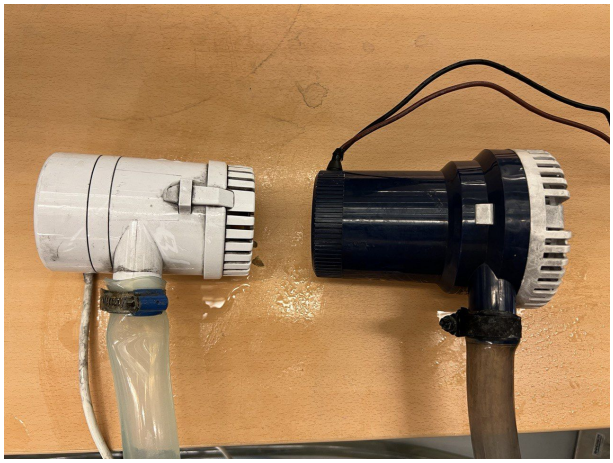

FIGURE D.7: Changing the pump

- Two LED panels were considered to improve the lighting. One was placed behind the pipe, and another was located in the front of the setup, as shown in the left picture in Figure D.8. After some runs, it was specified that the brightness

at the bottom of the setup was too much, and the fluid displacement could not be analyzed. Finally, the problem was solved by putting the LED panel on the floor (see the right picture in Figure D.8).

FIGURE D.8: LED panel position

Appendix E

PASCO graphs

Voltage and pressure versus time are recorded by the PASCO system. Voltage is used to control the imposed velocity, and absolute pressure is used to monitor the hydrostatic pressure due to fluid height in the pipe. The examples of the PASCO graph are shown in Figure E.1 to Figure E.3. Since the displacing fluid level must be constant for all experimental runs, the hydrostatic pressure is set to 117 bar for each case. It is seen that it takes some time before the voltage is set to the constant value. Also, increasing the voltage at the end of the graphs is due to opening the outlet valve to discharge the fluid when the experimental test is finished.

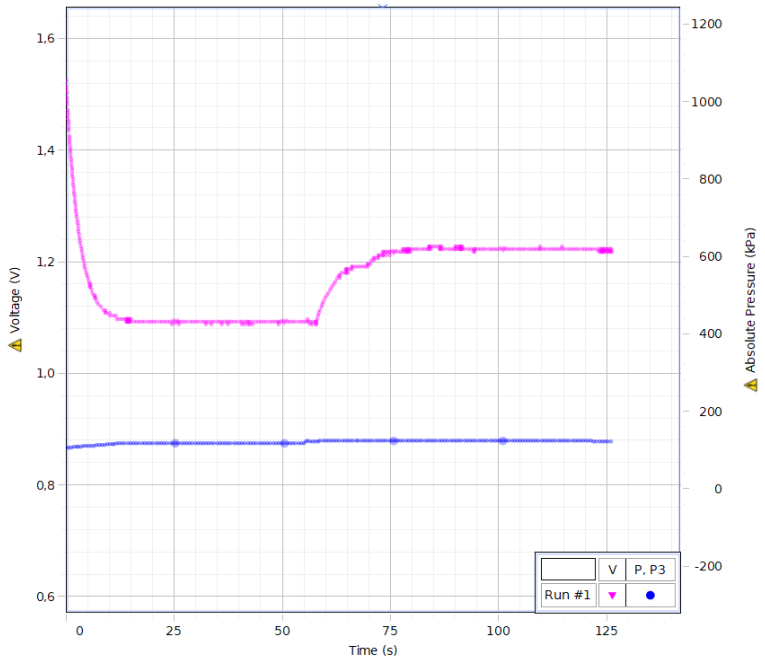

FIGURE E.1: PASCO graph for At = 0.003 and v = 12 mm/s

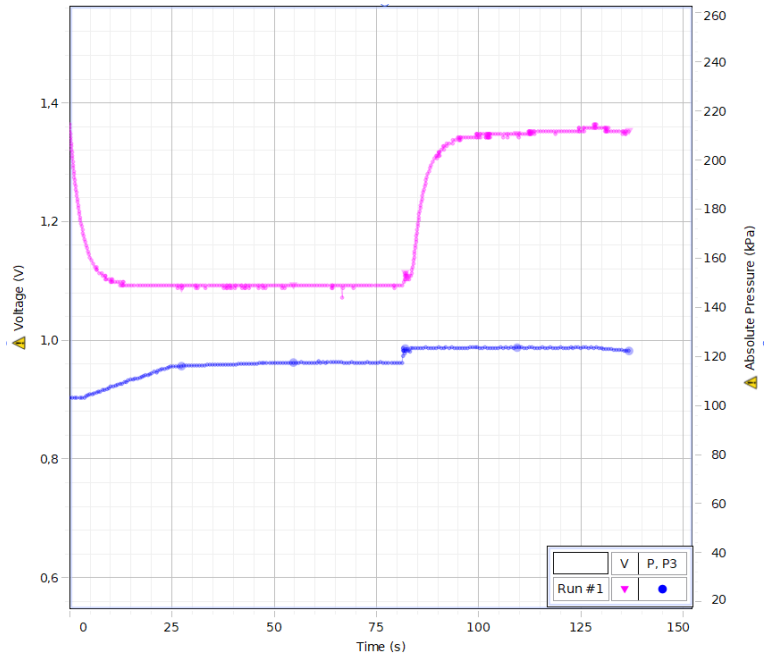

FIGURE E.2: PASCO graph for At = 0.003 and v = 25 mm/s

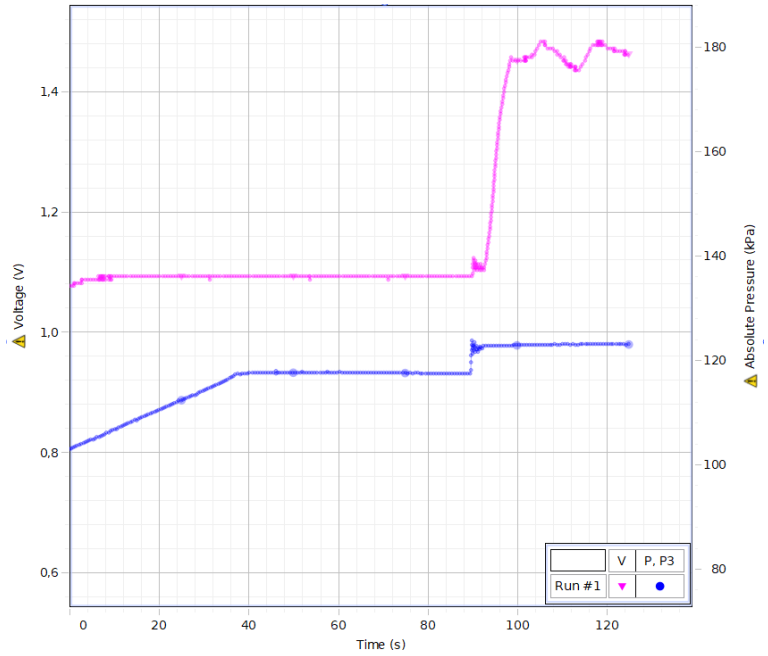

FIGURE E.3: PASCO graph for At = 0.02 and v = 33 mm/s

Appendix F

Python scripts

F.1 Video to frames

```
import cv2
vidcap = cv2.VideoCapture('case2-noflow.MOV')
success,image = vidcap.read()
count = 0
while success:
  cv2.imwrite("frames/%d.jpg" % count, image) # save frame
  as JPEG file
  success,image = vidcap.read()
  print('Read a new frame: ', success)
  count += 1
```

F.2 Image cropping

```
from pylab import *
from PIL import Image
#import numpy as np
import cv2

nstart=780 #start of test
nend=6890  #end of test
nt=nend-nstart    #number of frames

img0 = Image.open(r"frames/1.jpg") # read one frame to
measure the dimension
nx,ny= img0.size
print(nx,ny)

left=0.017*nx
top=0.383*ny
right=0.854*nx  #/// 1cm is about 0.013*nx
```

```
bottom=0.446*ny#### camera=0.07300.0.5
left1=0.055*nx          #/// top
top1=0.139*ny #///0.147
right1=0.817*nx         #/// top
bottom1=0.198*ny#/// left mirror=0.068
left2=0.062*nx           #///bottom0.076
top2=0.599*ny#/// bottom 0.686
right2=0.807*nx        #///bottom 0.918
bottom2=0.658*ny#/// right mirror=0.068 0.732
#cropping

for i in range (nstart,nend):
#****MIDDLE*****
  img = Image. open(r"frames/%s.jpg"%str(i))
  b=img.rotate(-0.45)
  middle=b.crop((left, top, right, bottom))
  middle.save('crop-images/middle/%s.jpg'%str(i-nstart))
nx1,ny1=middle.size

#****top***** right mirror
for i in range (nstart,nend):
  img = Image. open(r"frames/%s.jpg"%str(i))
  b=img.rotate(-0.32)
  top=b.crop((left1, top1, right1, bottom1))
  top_new=top.resize((nx1,ny1))
  top_new.save('crop-images/top/%s.jpg'%str(i-nstart))


for i in range (nstart,nend):
  #****bottom***** left mirror
  img = Image. open(r"frames/%s.jpg"%str(i))
  bb=img.rotate(0.2)
  bottom=bb.crop((left2, top2, right2, bottom2))
  #bottom=img.crop((left2, top2, right2, bottom2))
  bottom_new=bottom.resize((nx1,ny1))
  bottom_new.save('crop-images/bottom/%s.jpg'%str(i-nstart))

#bottom.show()

#for i in range (ny):
  #for j in range (nx): #traverses through height of the image

   # grey[i,j]= 0.2989 * img[i,j,0] + 0.5870 *  img[i,j,1] +
   0.1140 *  img[i,j,2] # RGB To gray scale


#array = np.array(grey, dtype=np.uint8)
#spatiotemporal= Image.fromarray(array)

#spatiotemporal.save('test2.png')
```

F.3 Calculation of front velocity and displacement time, and result plotting

```
from pylab import *
from PIL import Image
import numpy as np
import cv2
import os

img0 = cv2.imread("crop-images/middle/0.jpg") # reference
ny=img0.shape[0] #height of the image - width of the annulus
nx=img0.shape[1] #width of the image - height of the annulus

n=6100 #/// numer of frames
step=2 # ///
nt= range (n)
ntstp = nt[::step]
#print(sortedNames)
ntt=len(ntstp)


f=50/step # number of frames in one second

av = zeros((nx,ntt,3))
C_m = zeros((nx,ntt))
C_r = zeros((nx,ntt))
C_l = zeros((nx,ntt))
C_av = zeros((nx,ntt))
C = zeros((nx,ntt))
C_n = zeros((nx,ntt))
maxx_C = zeros(ntt)
maxx_C_sort = zeros(ntt)
outlet= zeros(ntt)
inlet= zeros(ntt)
D = zeros(nx)
out=zeros(ntt)
start_t=zeros(50)
start_inletfilled=zeros(50)
end_t=zeros(50)
print (ny,nx)
#alpha_lim = 0.02


##### middle
for i in range (0,ntt):
  img = cv2.imread('crop-images/middle/%s.jpg'%str(i*step))
#print (img.shape)
  for j in range (nx): #traverses through height of the image
    av[j,i,0]=sum(img[:,nx-j-1,0])/ny
    av[j,i,1]=sum(img[:,nx-j-1,1])/ny
```

```
    av[j,i,2]=sum(img[:,nx-j-1,2])/ny
    C_m[j,i]=255-(0.2989 * av[j,i,0] + 0.5870 *  av[j,i,1]
    + 0.1140 *  av[j,i,2]) # RGB To gray scale

av = zeros((nx,ntt,3))


##### top_ right mirror
for i in range (ntt):
  img = cv2.imread('crop-images/top/%s.jpg'%str(i*step))
#print (img.shape)
  for j in range (nx): #traverses through height of the image
    av[j,i,0]=sum(img[:,nx-j-1,0])/ny
    av[j,i,1]=sum(img[:,nx-j-1,1])/ny
    av[j,i,2]=sum(img[:,nx-j-1,2])/ny
    C_r[j,i]=255-(0.2989 * av[j,i,0] + 0.5870 *  av[j,i,1]
    + 0.1140 *  av[j,i,2]) # RGB To gray scale

av = zeros((nx,ntt,3))

##### bottom- left mirror
for i in range (ntt):
  img = cv2.imread('crop-images/bottom/%s.jpg'%str(i*step))
#print (img.shape)
  for j in range (nx): #traverses through height of the image
    av[j,i,0]=sum(img[:,nx-j-1,0])/ny
    av[j,i,1]=sum(img[:,nx-j-1,1])/ny
    av[j,i,2]=sum(img[:,nx-j-1,2])/ny
    C_l[j,i]= 255-(0.2989 * av[j,i,0] + 0.5870 *  av[j,i,1] +
    0.1140 *  av[j,i,2]) # RGB To gray scale
    C_av[j,i]= (C_r[j,i]+C_l[j,i])/2  # mean value
    of mirrors, just images in mirrors are used to
    cover 360 degree


L=0.7         # length of the annulus
dz=L/nx
zs = linspace(dz/2,L-(dz/2),nx)
endtime=ntt/f
dt=1/f
ts = linspace(0,endtime,ntt)


 #///// lighgt modification


fig1, ax = plt.subplots()
ax.plot(zs,C_av[:,1])

zf0 = int(round(0*nx))
zf1 = int(round(1*nx))
```

```
zpf = zs[zf0:zf1]
zp = polyfit(zpf,C_av[zf0:zf1,1],2)
ax.plot(zpf,polyval(zp,zpf),linewidth=2)

for j in range(nx):   #//// the first frame is used
       if zs[j] < zs[zf0]:
        D[j]=C_av[j,1]
       else:
        D[j]=C_av[j,1]-(zp[0]*((zs[j]-zs[zf0])**2))
         -(zp[1]*(zs[j]-zs[zf0]))#-zp[2]
ax.plot(zs,D)


for i in range (ntt):
   for j in range(nx):
       if zs[j] < zs[zf0]:
        C_n[j,i]=C_av[j,i]
       else:
        #C[j,i]=C_n[j,i]
        C_n[j,i]=C_av[j,i]-(zp[0]*((zs[j]-zs[zf0])**2))
         -(zp[1]*(zs[j]-zs[zf0]))#-zp[2]


# converting the range of concentration
for i in range (ntt):
   maxx_C[i]=max(C_n[:,i])


maxx_C_sort=sort(maxx_C)
maxx=sum(maxx_C_sort[ntt-100:])/100
print('vv',len(maxx_C_sort[ntt-100:]))
mean=sum(C_n[:,1])/nx
#mean=min(C_av[:,1])
print (mean,maxx)
for i in range (ntt):
 for j in range (nx):
    C[j,i]=(C_n[j,i]-mean)/(maxx-mean)
    #C_n[j,i]=C_av[j,i]/maxx



# //// time of displacement


for i in range (ntt):
  for j in range (100):
     inlet[i]=sum(C[nx-101:nx-1,i])/100
     outlet[i]=sum(C[0:100,i])/100
     break
```

```
#//// definition of a limitaion for displacmenet
max_inlet=max(inlet)
index_max_inlet=[index for index in range(len(inlet))
if inlet[index] == max_inlet]
max_inlet_mean=average(inlet[index_max_inlet[0]:])

max_outlet=max(outlet)
index_max_outlet=[index for index in range(len(outlet))
if outlet[index] == max_outlet]
max_outlet_mean=average(outlet[index_max_outlet[0]:])

alpha_lim_end_inlet=0.97*max_inlet_mean
alpha_lim_end_outlet=0.97*max_outlet_mean
alpha_lim_test=3*min(inlet)
print('alpha_lim_test', alpha_lim_test)
alpha_lim=0.035

for i in range (ntt): # strat time of dispalcement,
when the inlet in fully filled with heavy fluid
  if C[nx-1,i]> alpha_lim:
     time_start=i*dt
     ts_index=i
     break

for i in range (ntt):
  if inlet[i]>alpha_lim_end_inlet:
     time_start_d=i*dt
     tsd_index=i
     break


for i in range (ntt): #//// start time of injection
  if C[1,i]> alpha_lim:
     time_end=i*dt
     te_index=i
     break

for i in range (ntt):
  if outlet[i]>alpha_lim_end_outlet:
     time_end_d=i*dt
     ted_index=i
     break

print('time_start_f:', time_start,
'time_start_displacemnet:', time_start_d, 'time_end_f:'
, time_end, 'time_end_d:', time_end_d, 'time_displacement:
', time_end_d-time_start_d)
print('maxxx', max(C_av[:,te_index]))
 #///// Spatiotemporal diagram
fig2, ax2 = plt.subplots()
ts2=ts[0:te_index-ts_index]
```

```
pcolor(ts2,zs,C[:,ts_index:te_index], cmap='magma_r') # magma
colorbar()
xlabel('Time (s)')
ylabel('Z (m)')

cs= linspace(-0.05,1,50)
for i in range (50):
  start_t[i]=time_start
  start_inletfilled[i]=time_start_d
  end_t[i]=time_end_d

#for i in range (ntt):
 #out[i]=C[nx-1,i]-min(C[nx-1,:])
tdisplc, ax3 = plt.subplots()
ax3.plot(ts,inlet[:],color='blue',linewidth=0.7)
ax3.plot(ts,outlet[:],color='red',linewidth=0.7)
plot(start_t,cs,'--',color='grey',linewidth=0.7)
plot(start_inletfilled,cs,'--',color='grey',linewidth=0.7)
plot(end_t,cs,'--',color='grey',linewidth=0.7)
plt.text(time_start, 0.1, 'Start of displacement', size=9)
plt.text(time_start_d, 0.9, 'the inlet is filled', size=9)
plt.text(time_end_d, 0.9, 'End of displacement',size=9)
ax3.set_xlabel('Time(s)')
ax3.set_ylabel('Concentration')
tdisplc.legend(('inlet','outlet'))


# Calculate front velocity

front_position = zeros(ntt)

for i in range (ntt):
    for j,z in enumerate(zs):
        alpha = C[j,i]
        if alpha > alpha_lim:
            z0 =  zs[j-1]
            z1 = z
            a0 = C[j-1,i]
            a1 = alpha
            z_interp = z0 + ((alpha_lim - a0)/(a1 - a0))*(z1 - z0)
            front_position[i] = z_interp
            break


Vf =-1*(front_position[1:] - front_position[:-1])/dt
fig3, ax4 = plt.subplots()
ax5 = ax4.twinx()
ax4.plot(ts2,front_position[ts_index:te_index],linewidth=2)
ax2.plot(ts2,front_position[ts_index:te_index],'--',linewidth=1)
ntt2=len(ts2)
pf0 = int(round(0.4*ntt2))
```

```
pf1 = int(round(0.7*ntt2))
tpf = ts2[pf0:pf1]
p = polyfit(tpf,front_position[pf0+ts_index:pf1+ts_index],1)
ax4.plot(tpf,polyval(p,tpf), linewidth=2)
ax5.plot(ts2,Vf[ts_index:te_index],'--',color='grey',alpha=0.5)
matplotlib.pyplot.ylim(-0.1,0.3)
ax4.set_xlabel('Time (s)')
ax4.set_ylabel('Z (m)')
fig3.legend(('Front position','Curve fit'))
ax5.set_ylabel('Front velocity (m/s)')

print('Front velocity:',p[0],average(Vf[pf0:pf1]))
file = open ('Frontposition.txt','w')
context= str(front_position[ts_index:te_index])
file.write(context)
file.close()
show()


#array = np.array(av, dtype=np.uint8)
#spatiotemporal= Image.fromarray(array)

#spatiotemporal.save('spatiotemporal.png')
```